

The absence of Parkin in hTau mice leads to synaptic mitochondrial dysfunction, alterations to the synaptic proteome, and increased phosphorylated tau in the Hippocampus



L. Daniel Estrella, Xiaoke Xu, Collin White, Jane E. Manganaro, Lexi Sheldon, Trey Farmer, Kelly L. Stauch*

University of Nebraska Medical Center, College of Medicine, Department of Neurological Sciences, Omaha, NE, USA

ARTICLE INFO

Keywords:
 Tauopathy
 Phosphorylated Tau
 Parkin
 ParkinW402A
 Mitophagy
 Alzheimer's disease
 Synapse
 Synaptic mitochondria

ABSTRACT

Amongst the major histopathological hallmarks in Alzheimer's disease are intracellular neurofibrillary tangles consisting of hyperphosphorylated and aggregated Tau, synaptic dysfunction, and synapse loss. We have previously shown evidence of synaptic mitochondrial dysfunction in a mouse model of Tauopathy that over-expresses human Tau (hTau). Here, we questioned whether the levels or activity of Parkin, an E3 ubiquitin ligase involved in mitophagy, can influence Tau-induced synaptic mitochondrial dysfunction. Here, we generated novel mouse strains by crossing hTau mice with either Parkin knockout mice or mice expressing mutant Parkin (Parkin^{W402A}, shown to lead to constitutively active Parkin in vitro). We found that Parkin levels are increased in synaptic mitochondria isolates from hTau compared to WT mice, suggesting increased mitophagy; while Parkin^{W402A} surprisingly led to decreased levels of Parkin in hTau mice. Furthermore, we showed that absence of Parkin in hTau mice leads to synaptic mitochondrial dysfunction; however, Parkin^{W402A} did not show functional rescuing effects. When compared to WT, proteomic analyses of synaptosomes demonstrated that hTau mice display protein changes that predict alterations to pathways related to mitochondrial metabolism, synaptic long-term potentiation, and synaptic calcium homeostasis. Both the absence of Parkin and expression of Parkin^{W402A} led to distinct changes in the hTau mouse synaptic proteome. Finally, we showed that Parkin-null hTau mice have higher levels of phosphorylated Tau in the hippocampal *Dentate Gyrus*, with no observable changes in hTau mice expressing Parkin^{W402A}. The data presented here illustrate the protective role that Parkin plays under Tau-induced mitochondrial and proteomic alterations, particularly at the synaptic level.

1. Introduction

Alzheimer's Disease (AD) remains the most common neurodegenerative disorder and the leading cause of dementia, with the current number of worldwide cases estimated to triple by 2050 (Scheltens et al., 2021). AD is primarily characterized by the accumulation of extracellular amyloid plaques and intracellular neurofibrillary tangles (NFTs) composed of hyperphosphorylated and aggregated tau (Lane et al., 2018). NFT stage is a better correlate with dementia than plaques (Scholl et al., 2016; Therriault et al., 2021). A main pathological feature in AD is synaptic dysfunction and consequent synaptic loss, which lead to the observed cognitive dysfunction and memory loss (Chen et al., 2019; Koffie et al., 2011; Lecca et al., 2022). More specifically, previous reports have identified some of the synaptic mechanisms that are altered

during tauopathy disease state, including, but not limited to, autophagy (Birdsall and Waites, 2019), synaptic mitochondrial function (Trease et al., 2022), synaptic mitochondria quality control (Ashrafi et al., 2014; Pickett et al., 2018), and metabolic/energy-associated pathways (Hesse et al., 2019). During homeostatic conditions, synapses utilize large amounts of energy to properly function and maintain adequate neurotransmission (Li and Sheng, 2022). Thus, proper synaptic mitochondrial function is a key factor for maintaining synaptic function through ATP production for neurotransmitter vesicle release, synaptic plasticity, and the buffering of calcium ions during high neural activity (Duarte et al., 2023).

Mitophagy, a form of selective autophagy, is an essential mechanism that cells utilize for the turnover of damaged mitochondria, preventing their accumulation (Narendra and Youle, 2024). In preclinical models of

* Corresponding author at: Department of Neurological Sciences, University of Nebraska Medical Center, Omaha, NE 68198, USA.

E-mail address: kelly.stauch@unmc.edu (K.L. Stauch).

AD and AD-derived patient cells, mitophagy alterations have been reported, which coincide with an increase in the number of damaged mitochondria (Cummins et al., 2019). While mitophagy can occur through different pathways (Villa et al., 2018), pink1/parkin-mediated mitophagy has been shown to be altered in neurodegenerative disease, including Parkinson's disease and AD. For instance, the levels of parkin, an E3 ubiquitin ligase that tags mitochondria for lysosomal degradation, have been reported to be predominantly downregulated in the brains of both AD patients and preclinical models of AD (Henrique et al., 2021; Hu et al., 2016; Martin-Maestro et al., 2016). In the context of tau pathology, absence of parkin in mice overexpressing mutant human tau^{VLW/ VLW} have been shown to exacerbate mutant tau-induced protein aggregation and cognitive dysfunction (Menendez et al., 2006; Rodriguez-Navarro et al., 2008), which suggest that parkin may be protective in tauopathy. Despite these studies being in the context of mutant human tau, the influence that parkin has in non-mutant human tau pathology has not been reported.

The goal of this study was to determine if genetic ablation of parkin or expression of a mutant form of parkin, suggested to exhibit increased basal activity in vitro, in mice overexpressing non-mutant human tau (all six isoforms in the absence of murine tau, hTau mice) is deleterious or protective, respectively, with regards to synaptic mitochondrial dysfunction. Importantly, we have previously shown that mitochondria are dysfunctional in the synapses of hTau mice (Trease et al., 2022), which exhibit AD-relevant tau pathology (Andorfer et al., 2003). Furthermore, we aimed to uncover the synaptic pathways by which parkin modulation potentially imparts these functional effects. To accomplish this, we generated novel mouse strains by crossing hTau mice with parkin knockout (PKO) mice or mice expressing mutant parkin (Parkin^{W402A}, CRISPR/Cas9 generated Parkin^{W402A}, which partially abolishes autoinhibition and leads to increased basal activity of parkin in vitro (human parkin W403A) (Sauve et al., 2022; Tang et al., 2017; Trempe et al., 2013). We found that parkin and ubiquitin levels are increased in synaptic mitochondria isolates from hTau compared to WT mice, which was abolished with parkin deficiency, suggesting parkin is being recruited to dysfunctional synaptic mitochondria and tagging them for degradation by mitophagy in hTau mice. Furthermore, bioenergetic assessments showed that the absence of parkin in hTau mice led to impaired mitochondrial and glycolytic functions in synaptosomes; however, the mutant form of parkin (Parkin^{W402A}) did not seem to show rescuing effects. When compared to WT, proteomic analyses of synaptosomes demonstrated that hTau mice display protein changes that predict alterations to pathways related to mitochondrial metabolism, synaptic long-term potentiation, synaptic calcium homeostasis, and other relevant metabolic and signaling pathways. Both the absence of parkin and expression of Parkin^{W402A} led to further changes in the hTau mouse synaptic proteome, particularly those related to mitochondrial metabolism and synaptic plasticity. Finally, we show that parkin-null hTau mice have higher levels of phosphorylated tau in the hippocampal Dentate Gyrus, compared to hTau controls.

2. Materials & methods

2.1. Generation of novel hTau/PKO and hTau/Parkin^{W402A} mice

Congenic mice used for this study were generated by intercrossing human tau transgenic mice (hTau, JAX strain #005491, overexpress all six non-mutant human tau isoforms in the absence of murine tau) with either parkin knockout mice (PKO, JAX strain #006582) or mutant parkin mice (Parkin^{W402A}, Taconic strain #15143, now available as JAX strain #029317, CRISPR/Cas9 generated mice carrying mutant Parkin^{W402A}), then backcrossing the progeny to the hTau strain for a minimum of ten generations.

The hTau (Andorfer et al., 2003; Polydoro et al., 2009), PKO (Goldberg et al., 2003), and Parkin^{W402A} (Kim et al., 2022; Licher et al., 2023) mice have been described previously. To confirm the absence of

murine tau, we generated new genotyping primers as the original forward and reverse primer sequences from JAX detect the inserted eGFP cassette used to disrupt the murine *Mapt* gene in the tau KO mice (Tucker et al., 2001), which would also detect the inserted eGFP cassette used to disrupt the murine *Park2* gene in the PKO mice and as such, could not distinguish between tau KO and PKO mice. The new genotyping primers used to confirm tau KO included: 5' – CAGGCTTTGAACCAAGTATGG – 3', which was designed to anneal between the 52,957 and 52,976 base positions in the murine *Mapt* gene, and 5' – TGAACCTGTGGCCGTTACG – 3', which is complimentary to the eGFP cassette inserted a few base pairs ahead of murine *Mapt* gene (Supplemental Fig. 1A). The presence of the human MAPT transgene was confirmed using the JAX primers: oIMR3115 5' – ACTTTGAACCAGGATGGCTGAGCCC – 3' and oIMR3116 5' – CTGTGCATGGCTGTCCTACCTT – 3' (Supplemental Fig. 1B). The absence of parkin was confirmed using the JAX primers: oIMR7026 5' – CCTACACAGAACTGTGACCTGG – 3', oIMR7027 5' – GCAGAATTACAGCAGTTACCTGG – 3', and oIMR7028 5' – ATGTTGCCGTCCTCCTTGAAGTCG – 3' (Supplemental Fig. 1C). Lastly, the Parkin^{W402A} genotype was confirmed using the Taconic primers: Taconic #13156_3 5' – TTGAGCTTGCCCAAAGGC – 3' and Taconic #13156_4 5' – CCTTGAAACTGCTACTGCG – 3' (Supplemental Fig. 1D). For the Parkin^{W402A} genotyping, a *Xba*I restriction enzyme digestion (New England Biolabs, Ipswich, MA, USA) was performed on the genotyping PCR product for 2 h at 37 °C in order to identify the mutation knock-in (KI). Raw electrophoresis gels are provided in Supplemental File 1.

Male wild-type (WT, C57BL/6 J, JAX Strain #000664), hTau, hTau/PKO, and hTau/Parkin^{W402A} mice were aged to 8–9 months for all experiments. This age was chosen since at 8–9 months hTau mice exhibit tau pathology (Andorfer et al., 2003) and synaptic mitochondrial dysfunction (Trease et al., 2022). Tau pathology and synaptic mitochondrial function deficits were found in both male and female hTau mice; however, the previous study revealing synaptic dysfunction and cognitive impairments were performed using only male mice (Polydoro et al., 2009). Thus, for this study we chose male mice to test the effect of modulating parkin. The number of mice used per group (i.e., WT, hTau, hTau/PKO, and hTau/Parkin^{W402A}) was $n = 5\text{--}6$ for each experiment. Mice were housed in a temperature-controlled environment with 12-h light/dark cycle with free access to food and water in the Department of Comparative Medicine at UNMC. Experimental protocols were approved and conducted according to the University of Nebraska Medical Center Institutional Animal Care and Use Committee (IACUC) and under both the ARRIVE and the NIH guidelines for humane treatment of animals.

2.2. Immunohistochemistry

Mice from each experimental group were euthanized via cervical dislocation and decapitation at 8–9 months of age. Brain processing and slide staining was performed as previously described by our group (Lamberty et al., 2023). In brief, 50-μm thick hippocampal brain sections were collected using a vibrating microtome and subsequently stained with the following primary antibodies following Mouse-On-Mouse (M.O.M.) blocking treatment: total Tau (1:600, Cat #46687, Cell Signaling Technology, Danvers, MA, USA), AT8 (pTauSer202 + pTauThr205, 1:250, Cat #MN1020, Invitrogen, Waltham, MA, USA), PSD95 (1:1000, Cat #MA1-046 Invitrogen, Waltham, MA, USA), and synaptophysin (1:400, Cat #101006, Synaptic Systems, Göttingen, Germany). For secondary antibody conjugation, the following antibodies were used: Alexa Goat anti-Chicken 568 (1:1000, Cat #A11041, Invitrogen), Alexa Donkey anti-Mouse 647 (1:1000, Cat #A-31571, Invitrogen), Alexa Goat anti-Rabbit 488 1:1000, Cat #A11008, Invitrogen), and DAPI for nuclear counterstain.

Stained slides were imaged at the hippocampal Dentate Gyrus (DG), CA3, and CA1, as well as the medial and lateral parietal cortex (2 pictures per region) using a Nikon A1R upright confocal microscope under a 60×-oil immersion objective. Tau- and AT8- stained fluorescent

images were obtained at 1024×1024 pixel size (0.35- μm , 12 z-stack steps) with 561 and 640 nm lasers. Analysis of AT8/Total Tau co-occurrence was performed in ImageJ (Schindelin et al., 2012) by setting the total Tau color to green and AT8 to red. To measure the percent (%) area of co-occurrence and calculate the levels of p-Tau, a color threshold was set for only within the yellow color range (green + red co-occurrence = yellow) and the % area of such positive stains was quantified. We performed the quantification of excitatory synapses as previously described by our group (Daniel Estrella et al., 2025). In brief, to count the number of co-occurrences between synaptophysin (green) and PSD95 (red), individual maximum intensity z-stack channels were merged, and a consistent color threshold was set for only within the yellow color range (green + red co-occurrence = yellow). Then, the number of particles under that threshold and under a size inclusion of no smaller than 0.5- μm were quantified per each pictograph.

2.3. Synaptosome isolations

Upon euthanasia via cervical dislocation and decapitation, brains were removed, and the cerebellum and olfactory bulbs were discarded. Following this, the fore/hind brains underwent the nerve terminal (synaptosome) isolation protocol as previously described by our group (Trease et al., 2022) and the resulting synaptic protein contents were lysed in 4 % SDS/DTT and stored at -80 °C. Briefly, a small aliquot from each homogenized brain sample was collected and the rest of the homogenate was subjected to serial spins and synaptosomes were separated via discontinuous percoll-gradient density layering following ultracentrifuge spinning. Protein contents were then quantified using a Pierce 660 nm Protein Assay (Thermo Fisher Scientific, Waltham, MA, United States) with bovine and serum albumin standards and the addition of α -cyclodextrin for ionic compatibility.

2.4. Synaptic mitochondria isolations

Upon euthanasia via cervical dislocation and decapitation, brains were removed, and the cerebellum and olfactory bulbs were discarded. Following this, the fore/hind brains underwent the synaptic mitochondria isolation protocol as previously described by our group (Trease et al., 2022) and the resulting synaptic mitochondrial protein contents were lysed in 4 % SDS/DTT and stored at -80 °C. Similar to the synaptosome isolation in section 2.3, homogenates were subjected to serial spins and synaptic mitochondria were separated via discontinuous percoll-gradient density layering; however, the mitochondria were released from the synaptosomes by nitrogen cavitation. Protein contents were then quantified using a Pierce 660 nm Protein Assay (Thermo Fisher Scientific) with bovine and serum albumin standards and the addition of cyclodextrin for ionic compatibility.

2.5. Immunoblotting

Isolated fore/hind brain homogenates and synaptic mitochondria were lysed in 4 % SDS/DTT and quantified using a Pierce660 nm Protein Assay (Thermo Fisher). A total of 30 μg of brain homogenate protein and 30 μg of synaptic mitochondrial protein were independently loaded into Nu-PAGE Bolt 4–12 % gradient polyacrylamide gels using an MES/SDS buffer system (Life Technologies, Carlsbad, CA, United States) and transferred onto a nitrocellulose membrane using an iBlot2 instrument (Invitrogen, Waltham, MA, United States). Membranes were blocked for 1 h in 5 % fat-free milk dissolved in Tris buffered saline with 0.1 % Tween-20 (TBS-T). Subsequently, membranes were incubated for two nights at 4 °C while rocking using the following primary antibodies diluted in the 5 % blocking solution: Parkin 5C3 (1:500, Cat #865601, Biolegend, San Diego, CA, United States), Beta Actin (1:20000, Cat #AM1829B, VWR, Radnor, PA, United States), VDAC (1:2000, Cat #4661, Cell Signaling Technologies), ubiquitin (1:500, Cat #13–1600, Thermo Scientific), p62 (1:1000, Cat #PM045, MBL, Woburn, MA), and

LC3 (1:1000, Cat #PM036, MBL). Following primary antibody incubation, membranes were washed 3 × 10 min with 1xTBS-T and later incubated for 1 h at RT while rocking with secondary antibodies: goat anti-rabbit 800CW (P/N: 926–32,211, 1:20,000, Licor, Lincoln, NE, United States), goat anti-mouse 680CW (P/N: 926–680,070, 1:20,000, Licor, Lincoln, NE, United States), and HRP-linked anti-mouse secondary (1:500, Cat #7076P2, Cell Signaling Technologies). After secondary antibody incubation, membranes were once again washed 3 × 10 min with 1xTBS-T and imaged using an Odyssey imager (Licor) under the appropriate channels. For the Parkin immunoblots, an HRP-linked chemiluminescent reaction was performed by incubating the membrane for 5 min at RT with the SuperSignal West Pico Chemiluminescent Substrate kit (1:1 per bottle, Cat #34078, Thermo Scientific). Quantification of immunoreactivity was achieved using Image Studio software (Licor). Levels of Parkin were normalized to the corresponding loading control from each tissue fractionation. The widely used parkin antibody PRK8 is directed towards the C-terminus of parkin and the human W403A (mouse W402 A) mutation within this region of parkin disrupts PRK8 antibody binding (Stevens et al., 2023) precluding its use for samples from Parkin^{W402A} mice. Thus, to overcome this issue we used the Parkin 5C3 antibody, which is directed towards the N-terminus of parkin, and we report that this antibody is specifically detecting parkin, evidenced by appropriate band in WT and human parkin overexpressing mice, but lack of this band in PKO mouse samples (Supplemental Fig. 2A). Of note, the PKO mice used in this study were generated by insertion of a GFP cassette to disrupt the murine Park2 gene, and while the PRK8 antibody was used to confirm the absence of parkin in the PKO mice by Western blot (Goldberg et al., 2003), the PRK8 antibody epitope is lost in the resulting mutant truncated parkin protein (which consists of the N-terminal parkin residues 1–95 fused to the GFP protein (Goldberg et al., 2003)). Here using the Parkin 5C3 antibody we find that the mutant truncated parkin protein generated by insertion of the GFP cassette is present in the PKO mice (Supplemental Fig. 2A). Raw Western blots and corresponding Coomassie stained gels are provided in **Supplemental File 2**.

2.6. Synaptosome bioenergetic analyses

Synaptosomes were isolated as described in section 2.3 and functional bioenergetics were measured using the Seahorse XFe96 analyzer as previously described (Choi et al., 2009; Trease et al., 2022). 15 μg of synaptosomes were quantified using BCA Pierce and plated per well on a poly-D-lysine coated culture plate (Agilent, Santa Clara, CA, United States) and centrifuged at 2500 $\times g$ for 30 min at RT. Well volume was then brought to 175 μL with pre-warmed incubation media (3.5 mM KCl, 120 mM NaCl, 1.3 mM CaCl₂, 0.4 mM KH₂PO₄, 1.2 mM MgSO₄, pH 7.4) and supplemented with 4 mg/mL fatty acid free bovine serum albumin. Finally, 5 μL of incubation media containing pyruvate and glucose for a final concentration of 10 and 15 mM, respectively, were added to each well. The seahorse experiments were set up by having $n = 5$ –6 biological replicates from hTau controls and $n = 5$ –6 from each one of the corresponding crosses (hTau/PKO and hTau/Parkin^{W402A}), with all conditions having a total of $n = 6$ technical replicates within the Seahorse well plate. Both oxygen consumption rate (OCR) and extracellular acidification rate (ECAR) were measured to study changes in mitochondrial respiration and glycolysis, respectively.

2.7. Synaptosome mass spectrometry-based proteomics

2.7.1. Isolation of peptides and LC-MS/MS

Isolated synaptosomes from all the conditions were lysed in 4 % SDS/DTT and quantified using a Pierce 660 nm Protein Assay (Thermo Fisher). Individual peptides were eluted, analyzed, and searched by the University of Nebraska Medical Center Multiomics Mass Spectrometry Core Facility (RRID: SCR_012539).

Suspension-trapping (S-trap™) processing. Unless otherwise noted, all

chemicals were obtained by Sigma-Aldrich. S-trap™ Turbo plate (Protifi) was used for sample processing on an OT2 robot (OpenTrons). Briefly, each 50 µg from each sample was reduced with 10 mM tris(2-carboxyethyl) phosphine in a heater-shaker module for 15 min set at 55 °C at 1200 rpm, followed by alkylation with 20 mM iodoacetamide for 30 min in the dark at room temperature at 1200 rpm. 27.5 % phosphoric acid was used to acidify the proteins, then samples were diluted with 300 µL of S-Trap™ binding buffer (100 mM TEAB, 90 % methanol with pH 7.1). The samples were then loaded onto S-Trap™ Turbo plate and washed three times 2:1 chloroform: methanol and then three times with S-Trap™ binding buffer. 8 µg of Trypsin-LysC in 50 mM TEAB solution was added to the top of the S-Trap™ Turbo and then incubated at 37 °C for 2 h. Peptides were eluted serially with 50 mM TEAB, and 0.4 % aqueous formic acid with 0.04 % DDM (n-Dodecyl β-D-maltoside, GoldBio).

Mass spectrometry. Peptide samples were diluted to 0.2 µg/µL measured by a **Pierce Quantitative Fluorometric Peptide Assay** (Fisher Scientific) using a Varioskan LUX multimode microplate reader (ThermoFisher). The samples (5 µL; 1 µg per injection) were analyzed using a Vanquish™ NEO liquid chromatography (UPLC) system with a μPAC™ Neo 50 cm column coupled to an Orbitrap Astral mass spectrometer (Thermo Fisher Scientific). Data acquisition settings are listed in supplementary information (**Supplemental Table S1**). Sample sets spiked with an iRT synthetic peptide mixture were blocked and acquired in randomized order with digested *E. coli* injected immediately before and after every sixth sample to evaluate system performance. The consistency and reproducibility of the system performance were evaluated using QuiC (5.3.240326.57353).

MS data analysis. The data analysis workflow that was performed is summarized in **Supplemental Table S2**. Briefly, Raw files were searched using directDIA default settings in Spectronaut™ 19.2.240905.62635 (Biognosys, Switzerland). Search data were normalized using equalized medians and log₂ transformed using MSstats package (4.2.1) in R studio (R version 4.2.2). The comparisons that were performed included the log₂ fold changes between: hTau vs WT, hTau/PKO vs hTau, and hTau/Parkin^{W402A} vs hTau (**Supplemental File 3**). A total of 9297 proteins were detected in all comparisons.

2.7.2. Global analysis: Ingenuity pathway analysis

Global pathway analysis was performed for each of the comparisons in Ingenuity Pathway Analysis (IPA) using the log₂ fold change values of all identified proteins from all 3 comparisons given by MS Stats. The Comparison Analysis tools, particularly the IPA Metabolic Pathways and IPA Signaling Pathways options, were used to uncover the pathways that were predicted to be activated or inhibited across all the given comparisons. For the IPA Metabolic Pathways option, we applied a p-value cutoffs of >1.3 (-log₁₀) and z-score = 1 (absolute value) with no further filtering options. All of the identified metabolic pathways with their corresponding z-score values for each of the comparison can be found in **Supplemental File 4**. For the IPA Signaling Pathways option, we also applied a p-value cutoffs of >1.3 (-log₁₀) and z-score = 1 (absolute value). Filters were further applied under the Signaling Pathways tab to only detect pathways involved in apoptosis, cellular stress and injury, intracellular second messenger signaling, and neurotransmitters and other nervous system signaling. All of the identified signaling pathways with their corresponding z-score values for each of the comparison can be found in **Supplemental File 5**.

2.7.3. Global analysis: Gene set enrichment analysis

Gene Set Enrichment Analysis (GSEA) ([Subramanian et al., 2005](#)) was also implemented using the log₂ fold change values of all identified proteins from all 3 comparisons given by MS Stats. With the cluster-Profiler R package ([Wu et al., 2021](#)) (version: 4.14.3) and the gseGO function, the proteomic data was ranked by the log₂ fold change in descending order and used as input for analysis. The biological process in the gene ontology database (GO BP) was used for enrichment and the

cut-off was set as $p < 0.05$ to select significantly changed pathways. The other parameters in the gseGO function were set as default. The identified pathways with their corresponding enrichment scores were used for plotting, which reflect the degree to which a gene set is overrepresented at the top or bottom of a ranked list of genes. A sample R script used to generate the gseGO BP analyses can be found in **Supplemental File 6**. Individual GSEA GO BP results for each of the comparisons can be found in **Supplemental File 7**. Due to the large number of pathways that were detected in the hTau/Parkin^{W402A} vs hTau comparison, only the top 8 upregulated and top 8 downregulated pathways were used in the generated heatmaps.

2.7.4. Analysis of differentially expressed proteins (DEPs) using STRING

To identify differentially expressed proteins, we set 2 significance cutoff values including $p\text{-value} = 1.3$ (-log₁₀) and $z\text{-score} = 1$ (absolute value) for each of the comparison results, given by MS Stats (**Supplemental File 3**). After identification of DEPs, The STRING database ([Snel et al., 2000; Szklarczyk et al., 2023](#)) ([string-db.org](#)) was used for network analysis in each of the given comparisons (hTau vs WT, hTau/PKO vs hTau, and hTau/Parkin^{W402A} vs hTau). The significantly upregulated and downregulated proteins were independently uploaded to the database and the k-means clustering method was used under a high confidence interaction score (min. Interaction score = 0.7). All of the identified clusters for each of the comparisons can be found in **Supplemental File 10**. After cluster identification, we selected the top upregulated and top downregulated clusters based on the number of proteins that contributed to such results. We also selected, when applicable, one relevant upregulated and one relevant downregulated cluster from each of the comparisons to further analyze. After selection of the cluster to analyze, the Gene Ontology Biological Process (GO BP), KEGG, and Reactome databases were used to identify the most upregulated and downregulated pathways related to the selected clusters, based on the given strength score. The strength score represents the ratio between the number of proteins in a given network and the number of proteins expected to be annotated with this term in a random network of the same size. Each of the selected clusters with their corresponding GP BP, KEGG, and Reactome database results can be found in **Supplemental File 11**.

2.8. Statistical analyses

Statistical analyses were performed using GraphPad Prism 10 software and outliers were identified using a Tukey's fences outlier test ($k\text{-value} = 1.5$). One-Way ANOVA statistical tests with Tukey's post-hoc ($\alpha = 0.05$) were used in the immunoblotting and histological experiments to determine significant differences between the experimental groups (degrees of freedom reported in figure legend). Two-way ANOVA with Šidák's multiple comparisons was used for the Seahorse experiments to determine significant differences between the experimental groups under different mitochondrial drug treatments (degrees of freedom reported in Figure legends). In accordance with rigor and reproducibility, the investigators were blinded during the experiments and analyses, and animals were randomly assigned to each cohort.

3. Results

3.1. Absence of parkin in hTau mice impaired mitochondrial respiration and glycolysis in synaptosomes while expression of Parkin^{W402A} had no effects

Tau-induced mitochondrial dysfunction remains a widely studied pathology within neurodegenerative disorders, particularly in AD. Our group has previously shown that hTau mice have impaired mitochondrial respiratory function, particularly at the synapse ([Treas et al., 2022](#)). Since parkin plays a key role in proper mitochondrial quality control, we tested whether the absence of parkin or presence of a mutant form of parkin (Parkin^{W402A}) predicted to have increased basal activity

could exacerbate or protect against, respectively, the synaptic mitochondrial respiratory dysfunction observed in hTau mice. To do this, we performed the Seahorse XF Cell Mito Stress Test in synaptosomes isolated from 8 to 9-month male hTau, hTau/PKO, and hTau/Parkin^{W402A} mice and measured both the oxygen consumption rate (OCR, mitochondrial respiration) and extracellular acidification rate (ECAR, glycolysis). In line with our hypothesis, the absence of parkin in hTau mice led to a significant decrease in maximal synaptic mitochondrial respiration (Fig. 1A and B). However, the presence of Parkin^{W402A} had no effects on synaptic mitochondrial respiration in hTau mice (Fig. 1C and D). While we observed reduced maximal glycolytic function in synaptosomes from hTau/PKO compared to hTau mice (Fig. 1E and F), no significant differences in glycolytic function were found in hTau/Parkin^{W402A} compared to hTau mice (Fig. 1G and H). Altogether, the findings presented here reveal parkin deficiency impairs maximal mitochondrial respiratory and glycolytic function in synaptosomes from hTau mice, suggesting parkin-mediated mitochondrial quality control, or other parkin-dependent pathways, are integral to protecting synaptic metabolism from tau-induced dysfunction. In contrast to our prediction, the mutant form of parkin (Parkin^{W402A}), shown to exhibit increased basal activity from in vitro studies of the corresponding human Parkin^{W403A} mutation (Tang et al., 2017; Yi et al., 2019), had no protective effects on synaptic mitochondrial respiratory function.

3.2. Synaptic mitochondria from hTau mice exhibited increased association of parkin while expression of Parkin^{W402A} in hTau mice decreased parkin levels

Since we found unexpected results in the Seahorse experiments for the hTau/Parkin^{W402A} mice, we measured the levels of parkin protein in brain homogenate and synaptic mitochondria lysates from WT, hTau, and hTau/Parkin^{W402A} mice. Our findings demonstrated that, the protein levels of parkin in the brain are significantly reduced in hTau mice, compared to WT (Fig. 2A and C). Interestingly, expression of Parkin^{W402A} in hTau mice led to a further decrease in parkin protein levels in the brain compared to both hTau and WT mice (Fig. 2A and C). Synaptic mitochondria from hTau mice had significantly higher levels of parkin protein compared to WT mice (Fig. 2B and D). Compared to hTau mice, expression of Parkin^{W402A} in hTau mice led to significantly lower levels of parkin in synaptic mitochondria lysates, which were not statistically different from parkin levels in the synaptic mitochondria isolated from the WT mice (Fig. 2B and D). We note animal-specific variations in parkin protein levels at the level of the whole brain as well as in synaptic mitochondrial isolates via Western blotting, which was also found in synaptosomes via mass spectrometry (described below) albeit to varying degrees (Supplemental Fig. 3B). In particular, we found a trend of increasing variability from WT to hTau to hTau/Parkin^{W402A} for parkin levels in both synaptosomes and brain, while in contrast we found the opposite trend for synaptic mitochondria with decreasing variability from WT to hTau to hTau/Parkin^{W402A}. This highlights the highly dynamic nature of parkin recruitment and parkin-mediated mitochondrial turnover (Ordureau et al., 2018). Taken together, our findings suggest that parkin is recruited to dysfunctional synaptic mitochondria in hTau mice to enable parkin-mediated mitochondrial quality control. Further, partial loss of autoinhibition of parkin (via W402A mutation) in vivo may trigger a response that leads to either the downregulation of parkin expression or an increase in parkin turnover, potentially confounding the use of Parkin^{W402A} expression in vivo to study induction of parkin activity as a protective strategy. To extend these findings, we assessed the levels of ubiquitin in synaptic mitochondria isolates from WT, hTau, hTau/PKO, and hTau/Parkin^{W402A} mice and found increased ubiquitination of synaptic mitochondria from hTau vs WT, hTau vs hTau/PKO, and hTau vs hTau/Parkin^{W402A} mice (Fig. 2E and F), suggesting dysfunctional synaptic mitochondria in hTau mice are being tagged for degradation and parkin is essential for the increased ubiquitination observed in the hTau mice.

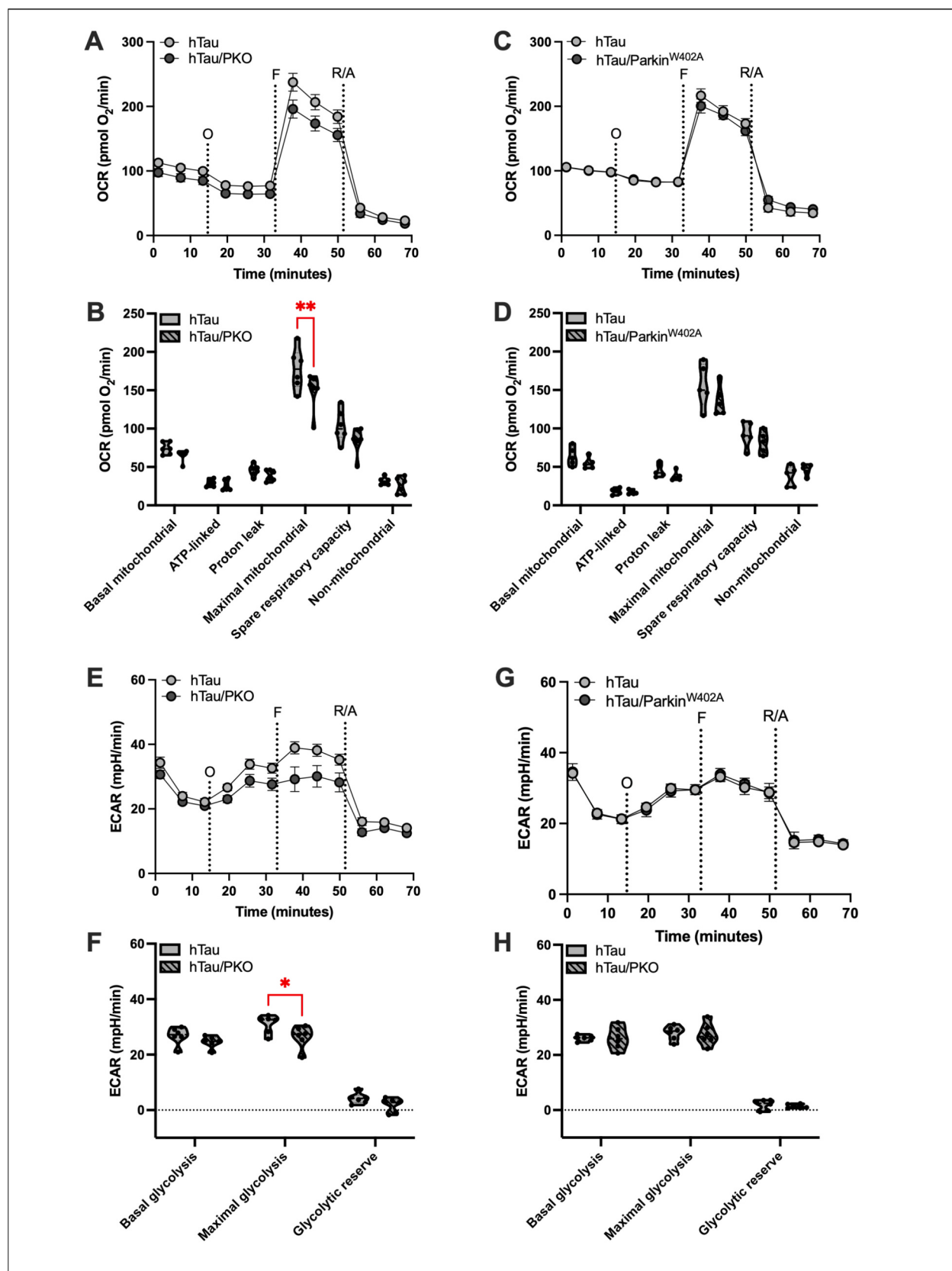
This effect may be specific to the neuronal synapse as we did not observe any significant changes in the levels of the mitochondrial marker VDAC nor the autophagy markers p62 and LC3 (unaltered LC3-II to LC-1 conversion) in brain homogenates from the different mouse groups (Supplemental Fig. 3), indicating mitochondrial mass and autophagic flux may be unaltered overall in the brain. Previously, we showed that mitochondrial content at the synapse is unaltered in hTau as compared to WT mice (Trease et al., 2022). Here, our synaptosome proteomics (described below) validates that finding and reveals parkin absence or presence of Parkin^{W402A} does not alter mitochondrial content at the synapse (no significant protein expression level differences were found for mitochondrial marker proteins or mitochondrial DNA-encoded proteins between the mouse groups (Supplemental Fig. 4)). This is further supported by our findings that basal mitochondrial respiration is unaltered between the mouse groups in isolated synaptosomes (Fig. 1).

3.3. Quantitative synaptosome proteomics identified changes to molecular networks and pathways that were differentially regulated by parkin in hTau mice

3.3.1. Ingenuity pathway analysis uncovered altered metabolic and signaling pathways at the synapse in hTau mice and revealed which pathways were influenced by parkin

We found increased levels of parkin associated with synaptic mitochondria from hTau mice (Fig. 2) and that parkin deficiency led to synaptosomal bioenergetic dysfunction in hTau mice (Fig. 1). To uncover the mechanisms underlying these functional changes, we performed mass spectrometry-based quantitative proteomics using data-independent acquisition (DIA) on the isolated synaptosome samples from the 8–9-month-old male WT, hTau, hTau/PKO, and hTau/Parkin^{W402A} mice ($n = 5$ mice per group). In total, 9297 proteins were identified and the complete list of these proteins with quantitative values is provided in **Supplemental File 3**. Functional annotation analysis of the proteomics data was conducted using Ingenuity Pathway Analysis (IPA). Comparison Analysis was performed using IPA to visualize the \log_2 protein expression changes to identify global proteomic similarities and differences between the synaptosomes from the different mouse strains (\log_2 hTau vs WT, \log_2 hTau/PKO vs hTau, and \log_2 hTau/Parkin^{W402A} vs hTau).

The Metabolic Pathway Analysis revealed differential alterations in multiple pathways within hTau mice (Fig. 3A and **Supplemental File 4**). “Oxidative Phosphorylation” in particular, had the strongest positive activation z-score (3.536) for hTau vs WT mice predicting activation of this pathway in synaptosomes. In the absence of parkin, an exacerbation of this effect was observed as the activation z-score for “Oxidative Phosphorylation” was also positive (1.376) for hTau/PKO vs hTau mice. This suggests compensatory protein expression changes, as we reported impaired synaptic mitochondrial respiration in hTau mice (Trease et al., 2022) and the exacerbation of this in hTau mice lacking parkin (Fig. 1). In line with our findings of unaltered synaptic mitochondrial respiration in hTau/Parkin^{W402A} compared to hTau mice (Fig. 1), expression of Parkin^{W402A} in hTau mice was not predicted to activate nor inhibit “Oxidative Phosphorylation” in synaptosomes. Metabolic Pathway Analysis revealed “Phosphatidylglycerol Biosynthesis II (Non-plastidic)” had the strongest negative activation z-score (-2.4) for hTau vs WT mice. Phosphatidylglycerol functions as a lipid precursor in the biosynthesis of cardiolipin, which is an essential lipid in charge of maintaining inner mitochondrial membrane potential and membrane structure (Tracey et al., 2018). Thus, our results suggest that the synaptic mitochondria may have reduced cardiolipin levels in hTau mice, which is relevant as decreased levels of cardiolipin are associated with AD (Monteiro-Cardoso et al., 2015). While parkin deficiency in hTau mice did not predict the activation or inhibition of “Phosphatidylglycerol Biosynthesis II (Non-plastidic)”, expression of Parkin^{W402A} in hTau mice led to the opposite effect on this pathway as the activation z-score was positive (1.147) for hTau/Parkin^{W402A} vs hTau mice, suggesting a



(caption on next page)

Fig. 1. Parkin deficiency impairs maximal mitochondrial respiration and glycolytic function in synaptosomes from hTau mice. The Seahorse XF Cell Mito Stress Test was performed using synaptosomes isolated from 8 to 9-month-old male hTau, hTau/PKO, and hTau/Parkin^{W402A} mice. Oxygen consumption rate (OCR) line graphs for (A) hTau/PKO and (C) hTau/Parkin^{W402A} compared to hTau mice. Line graph data presented as mean \pm SEM. Calculated respiration profiles for (B) hTau/PKO and (D) hTau/Parkin^{W402A} compared to hTau mice. Significance: $p < 0.01^{**}$, two-way ANOVA (hTau/PKO vs hTau: interaction DF = 5, respiration profiles DF = 5, genotype DF = 1, and residual DF = 60; hTau/Parkin^{W402A} vs hTau: interaction DF = 5, genotype DF = 1, and residual DF = 48) followed by Šidák's multiple comparisons test. $n = 5\text{--}6$ mice per group. Extracellular acidification rate (ECAR) line graphs for (E) hTau/PKO and (G) hTau/Parkin^{W402A} compared to hTau mice. Calculated glycolytic profiles for (F) hTau/PKO and (H) hTau/Parkin^{W402A} compared to hTau mice. Significance: $p < 0.05^*$, two-way ANOVA (hTau/PKO vs hTau: interaction DF = 2, respiration profiles DF = 2, genotype DF = 1, and residual DF = 30; hTau/Parkin^{W402A} vs hTau: interaction DF = 2, respiration profiles DF = 2, genotype DF = 1, and residual DF = 30) followed by Šidák's multiple comparisons test. $n = 5\text{--}6$ mice per group. Violin plot data presented with median and quartiles indicated with dashed lines. DF = degrees of freedom; O = oligomycin, complex V inhibitor; F = FCCP, uncoupler; R/A = rotenone/antimycin A, complex I/III inhibitors.

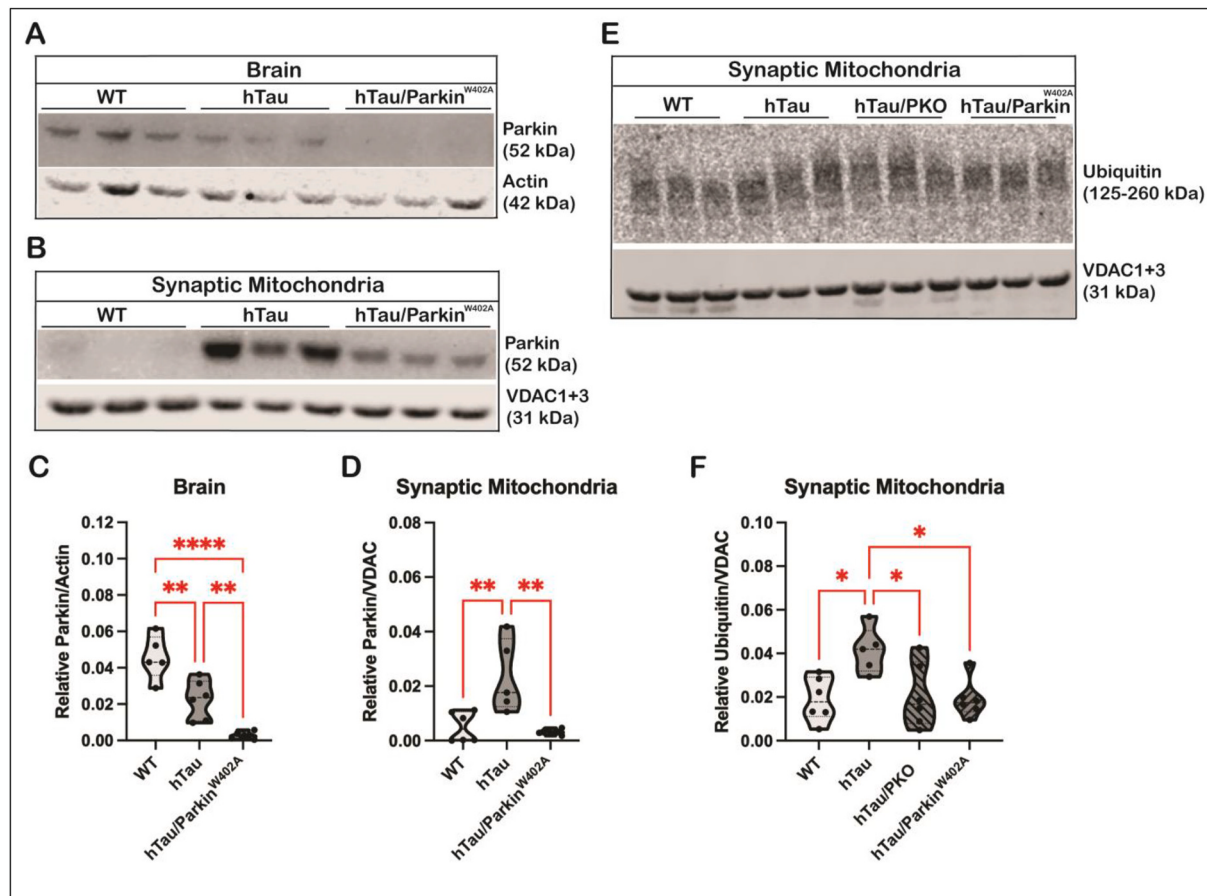


Fig. 2. hTau mice synaptic mitochondria display increased levels of parkin and ubiquitination. Brain homogenate and synaptic mitochondria were isolated from 8 to 9-month-old WT, hTau, hTau/PKO, and hTau/Parkin^{W402A} mice to assess the levels of select proteins using immunoblotting. Representative immunoblots for parkin in (A) brain and (B) synaptic mitochondria as well as (E) ubiquitin in synaptic mitochondria along with their corresponding loading controls (actin for brain, VDAC1 + 3 for synaptic mitochondria). Quantification of the levels of parkin in (C) brain homogenate (normalized to actin) and in (D) synaptic mitochondria (normalized to VDAC1 + 3) as well as (F) ubiquitin in synaptic mitochondria (normalized to VDAC1 + 3). Significance: $p < 0.05^*$, 0.01^{**} , one-way ANOVA (Brain (parkin): genotype DF = 2, and residual DF = 15; synaptic mitochondria (parkin): genotype DF = 2, and residual DF = 14; synaptic mitochondria (ubiquitin): genotype DF = 3, and residual DF = 19) followed by Tukey's multiple comparisons test. $n = 5\text{--}6$ mice per group. Violin plot data presented with median and quartiles indicated with dashed lines. DF = degrees of freedom.

partial restoration towards WT mouse activity. The absence of parkin in hTau mice also led to distinct metabolic changes, when compared to hTau mice. For instance, "Ketolysis" had the strongest positive z-score value (2.449), predicting the activation of this pathway which could potentially lead to an augmentation in synaptic energy production that could be related to the observed increase in "Oxidative Phosphorylation" (1.376). On the other hand, "D-myo-inositol-5-phosphate Metabolism" was predicted to be inhibited with the strongest negative z-score (-2.83) in hTau/PKO mice, when compared to hTau mice. Interestingly, alterations to the myo-inositol metabolic pathway have been found in postmortem AD brains (Shimohama et al., 1998) and inositol phosphates have also been found to influence tau phosphorylation (Randez-

Gil et al., 2020). Regarding hTau/Parkin^{W402A} synaptosomes, the metabolic pathway with the strongest positive z-score (3.638), when compared to hTau mice, was "Glycolysis I". Of note, alterations to the glycolytic pathway were in fact not detected in our synaptosome Seahorse experiments (Fig. 1), using extracellular acidification rate to compare glycolytic function between hTau/Parkin^{W402A} and hTau mice. This contradiction may be due to the difference in the experimental approaches that were taken to infer glycolytic function (Seahorse ECAR vs Protein Expression). For instance, Seahorse ECAR provides indirect evidence for glycolytic function by measuring the pH level changes that are attributed to the conversion of lactate to hydrogen, rather than to pyruvate. On the other hand, the results shown by the synaptosomal

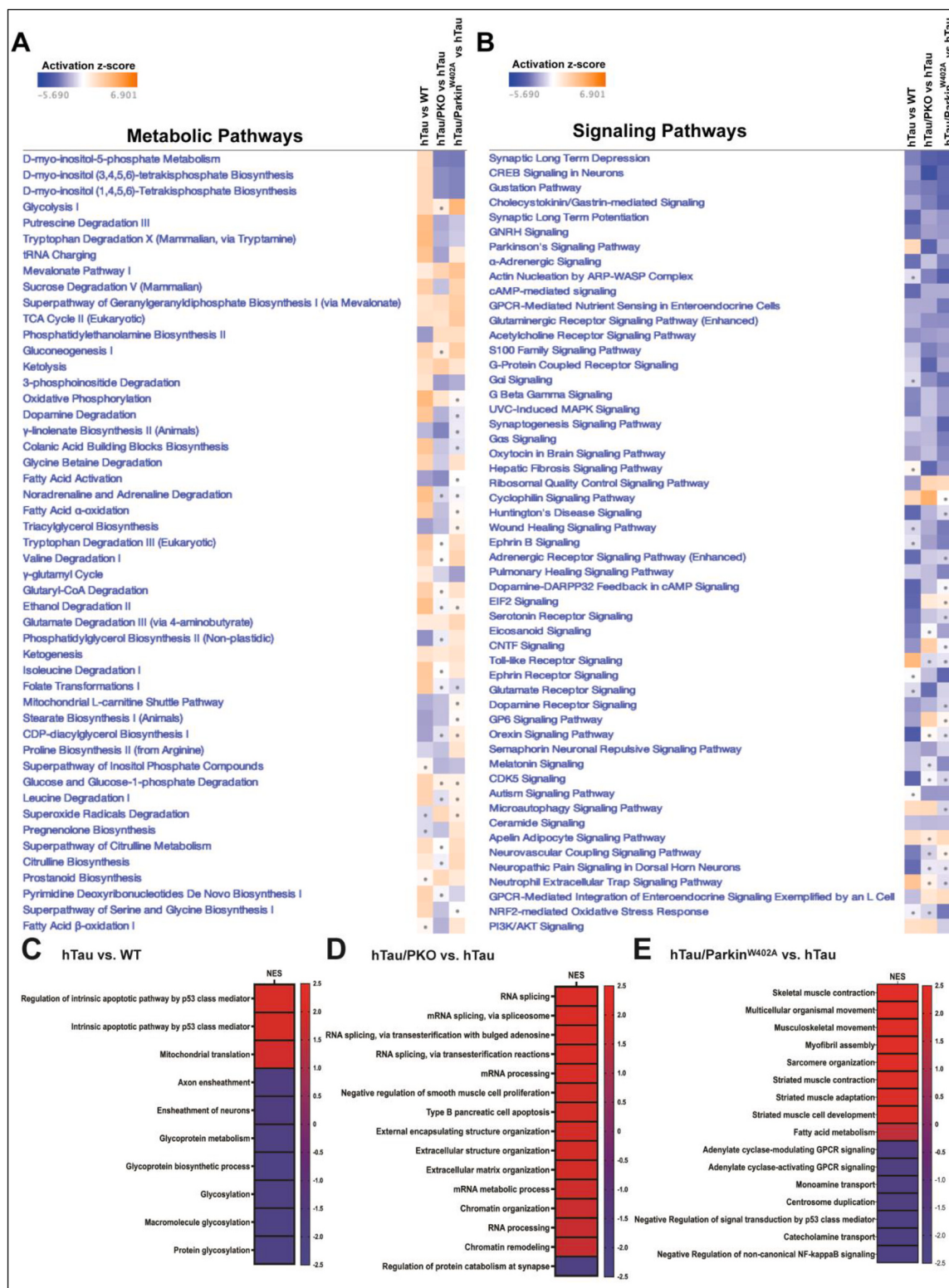


Fig. 3. Global analysis of synaptosome proteomics using Ingenuity Pathway Analysis (IPA) and Gene Set Enrichment Analysis (GSEA). Heatmap representing enriched (A) metabolic and (B) signaling pathways produced by IPA canonical pathway analysis comparing all the studied conditions. Score filter p-value cutoff = 1.3 (log10) and z-score cutoff = 1 (absolute value). Blue blocks and orange blocks represent inhibited and activated pathways, respectively. Gray dots represent pathways that did not achieve significance in the given experimental comparison. Heatmaps show the GSEA enrichment scores (NES) and adjusted p-value for the identified Gene Ontology Biological Processes (GO BP) that were significantly changed in (C) hTau vs WT, (D) hTau/PKO vs hTau, and (E) hTau/Parkin^{W402A} vs hTau synaptosomes. n = 5 mice per group. Enrichment analysis was performed in the R software using a p-value cutoff of <0.05. The Benjamini–Hochberg postdoc test was then applied for the generation of adjusted p-values. (For interpretation of the references to color in this figure legend, the reader is referred to the web version of this article.)

proteomics indirectly report changes to the glycolysis pathway based on the expression levels of proteins that are known to be related in such metabolic pathway. Similar to parkin-null hTau mice, “D-myo-inositol-5-phosphate Metabolism” was predicted to be inhibited in hTau/Parkin^{W402A} mice and had the strongest negative z-score (-2.83), when compared to hTau mice. The latter further provides evidence of the similarities that exist between the effects that the absence of parkin and Parkin^{W402A} have in the hTau brain, particularly at the synapse.

The Signaling Pathway Analysis also revealed differential alterations in multiple pathways between the different mouse strains (**Fig. 3B and Supplemental File 5**). Here, the pathway with the strongest positive activation z-score (3.545) in hTau vs WT mice was “Toll-like Receptor (TLR) signaling”. This suggests TLR signaling, which can be present both in neuronal and neuro-glial synapses and can influence inflammatory responses, is predicted to be activated in hTau mice. Neither the absence of parkin nor presence of Parkin^{W402A} in hTau mice were predicted to significantly influence the activation of “TLR signaling” in synaptosomes. Further, Signaling Pathway Analysis demonstrated that the “Orexin pathway” had the strongest negative z-score (-3.919) for hTau vs WT mice and as such was predicted to be inhibited. This was an unexpected result as orexin pathway activation has been linked to AD-related sleep disturbances and increased proteinopathy (Zhou and Tang, 2022). Neither the absence of parkin nor expression of Parkin^{W402A} in hTau mice had an effect on the inhibition of the “Orexin pathway”. Interestingly, “Synaptic Long-Term Potentiation (LTP)”, an essential pathway involved in synaptic plasticity, had the second strongest negative activation z-score (-3.58) in hTau vs WT mice. Here, both the absence of parkin and expression of Parkin^{W402A} in hTau mice led to an exacerbation of this effect with both showing a negative activation z-score for “Synaptic Long-Term Potentiation” (hTau/PKO vs hTau = -1.964, hTau/Parkin^{W402A} vs hTau = -2.305). These results predict an inhibition of synaptic plasticity in hTau mice that is further impaired by the absence of parkin and expression of Parkin^{W402A}. The absence of parkin in hTau mice also led to the predicted activation of distinct signaling pathways, when compared to hTau mice. Interestingly, the “Cyclophilin Signaling Pathway” had the strongest positive activation z-score (3.984) in hTau/PKO mice, when compared to hTau mice. Cyclophilin D in particular, a type cyclophilin involved in the mitochondrial permeability transition pore, has been implicated in Alzheimer’s disease and it has been shown to regulate disease pathology by interacting with amyloid beta and exacerbating mitochondrial bioenergetic dysfunction, synaptic plasticity alterations, and learning/memory deficits (Du et al., 2008; Samanta et al., 2024). Importantly, the signaling pathway that had the strongest negative z-score (-4.518) was “CREB Signaling in Neurons”, which plays an important role in maintaining synaptic plasticity and has been shown to be altered in AD (Saura and Valero, 2011). Furthermore, “CREB Signaling in Neurons” was also predicted to be inactivated in hTau mice, when compared to WT (-2.293), demonstrating that the absence of parkin leads to further inactivation of this pathway, potentially exacerbating the initial hTau-induced effects. In the hTau/Parkin^{W402A} vs hTau comparison, the pathway that was predicted to be activated with the strongest z-score (2.201) was “PTEN Signaling”, which is a known negative regulator of insulin/phosphoinositide 3-kinase signaling and stimulation of this pathway correlates with increased tau phosphorylation (Chen et al., 2012; Gupta and Dey, 2012). We previously mentioned that LTP is predicted to be inactivated in hTau mice and that both the absence of parkin and expression of Parkin^{W402A} further exacerbate these hTau-induced effects. Here, long-term-depression (LTD), another essential pathway involved in synaptic plasticity, showed the strongest negative z-score in the hTau/Parkin^{W402A} vs hTau comparison (-3.849). Importantly, hTau mice also displayed inactivation of LTD (-2.746), when compared to WT mice, and the absence of parkin in hTau mice also led to exacerbated inactivation (-3.606), just as observed in hTau/Parkin^{W402A} mice.

Taken together, functional annotation of the global proteomic

changes in synaptosomes from hTau vs WT mice revealed vast alterations in both metabolic and signaling pathways relevant to the function of neurons, synaptic plasticity, and neurotransmission, many shown to be altered in neurodegenerative diseases. Furthermore, we showed that modulation of parkin levels in hTau mice is a potential strategy to differentially regulate many of the identified pathways.

3.3.2. Gene set enrichment analysis: Gene ontology biological process analyses of the synaptic proteome identified distinct pathways are altered in hTau, hTau/PKO, and hTau/Parkin^{W402A} mice

To further study the synaptic proteomic alterations in hTau mice and the global effects of parkin modulation, we utilized the Gene Set Enrichment Analysis (GSEA) tool. Using the protein log₂ fold changes and p-values for the hTau vs WT, hTau/PKO vs hTau, and hTau/Parkin^{W402A} vs hTau comparisons obtained using MSstats (**Supplemental File 3**), GSEA analysis was performed in order to rank all 9297 quantified proteins for each comparison and identify the affected pathways using the Gene Ontology Biological Process (GO BP) database (**Supplemental File 7**).

In the hTau vs WT comparison, the pathway with the strongest positive Normalized Enrichment Score (NES), which reflects the degree to which a gene set is overrepresented at the top or bottom of a ranked list of genes, was the “Regulation of Intrinsic Apoptotic Signaling Pathway by p53 Class Mediator” (NES = 0.788, **Fig. 3C**). This suggests cellular stress is present in hTau mice and may induce changes to the p53 pathway, which upon activation, can lead to p53 translocation to the mitochondrial membrane, inducing the intrinsic apoptotic cascade that results in caspase-mediated cellular death (Vaseva et al., 2012). GSEA analysis of hTau mice with parkin deficiency or expressing Parkin^{W402A} did not identify the “Regulation of Intrinsic Apoptotic Signaling Pathway by p53 Class Mediator” as an affected pathway (**Fig. 3D-E**). On the other hand, the pathway that was predicted to be inhibited with the strongest negative NES in hTau, when compared to WT mice, was “Macromolecule Glycosylation” (NES = -0.569, **Fig. 3C**), an important post-translational modification that can lead to improper protein functioning when disrupted. Similarly, GSEA did not identify “Macromolecule Glycosylation” as an affected pathway in the absence of parkin or under Parkin^{W402A} (**Fig. 3D-E**).

In the GO BP results from the hTau/PKO vs hTau comparison, the pathway with the strongest positive NES was “RNA splicing” (NES = 0.577, **Fig. 3D**). While not expected at the synapse, this pathway was likely predicted to be activated due to the individual proteins that were identified and known to be involved in “RNA splicing”. However, mRNA binding proteins, which are involved in RNA splicing, have been reported to be influenced by synaptic activity and be able to translocate to the synapse for local mRNA translation (Liu-Yesucevitz et al., 2011). The only pathway that showed a negative NES was the “Regulation of Protein Catabolic Process at the Synapse” (NES = -0.889, **Fig. 3D**), which was primarily driven by changes in Rab26 and parkin protein levels (**Supplemental File 7**). The latter result suggests that hTau/PKO mice may experience alterations to protein turnover at the synapse, which could influence synaptic function.

The hTau/Parkin^{W402A} vs hTau comparison showed “Skeletal Muscle Contraction” as the pathway with the strongest positive NES (NES = 0.859, **Fig. 3E**), likely due to the high number of calcium-related proteins that were changed and that are known to contribute to such pathways. Interestingly, the pathway with the strongest negative NES in this comparison analysis was the “Negative Regulation of Non-Canonical NF-KappaB Signal Transduction” (NES = -0.802, **Fig. 3E**), which would suggest alteration to synaptic function and synaptic plasticity.

Taken together, we report that each GSEA comparison analysis (hTau vs WT, hTau/PKO vs hTau, and hTau/Parkin^{W402A} vs hTau) led to distinct GO BP changes that influence synaptic function and could be implicated in disease. However, we note that the GSEA analysis includes all GO BP pathways enriched in our proteomic dataset even if they are

not expected to be present at the synapse, and as described above, in such event the focus should be directed towards the individual protein changes that contributed to those pathways.

3.3.3. Functional annotation of the differentially expressed proteins in the synaptosomes of hTau mice and the regulatory role that parkin plays in these

To identify the differentially expressed proteins (DEPs) in the synaptosomes from hTau vs WT, hTau/PKO vs hTau, and hTau/Parkin^{W402A} mice, we employed a ratio threshold in addition to a *p*-value threshold. To obtain *p*-values, MSstats was used for statistical analysis, using *p* < 0.05 (adjusted) for the threshold (Supplemental File 3). The ratio threshold was determined from the normal distribution fit using 1 standard deviation (Supplemental Fig. 7). Thus, the absolute value of the z-score (normalized log₂ ratios) had to be superior to 1.0 (absolute value). Combining these thresholds, for the hTau vs WT comparison, a total of 333 DEPs were found, 149 upregulated and 184 downregulated (Fig. 4A). Interestingly, and in line with our immunoblotting data (Fig. 2A and C), parkin (Prkn) was found to be significantly upregulated in the synaptosomes from hTau mice compared to WT (Fig. 4A). While tau was quantified and not significantly different between hTau and WT, it is important to consider that less unique peptides that are shared between the mouse and human tau protein are available for identification as compared to human-to-human tau. When testing the number of shared unique peptides between the human and mouse peptide sequences using Expasy-PeptideMass (https://web.expasy.org/peptide_mass/), only 35.4 % of possible human trypsin cleaved tau peptides were found to be shared with mouse tau peptides (Supplemental File 8). Thus, the low percentage of shared unique tau peptides between WT and hTau could have potentially hindered the ability to identify changes in tau protein expression. Indeed, we have previously shown that tau protein levels are increased in synaptosomes from hTau compared to WT mice by immunoblotting (Trease et al., 2022). For the hTau/PKO vs hTau comparison, a total of 327 DEPs were found, 179 upregulated and 148 downregulated (Fig. 4B). As expected, we found parkin to be amongst the significantly downregulated proteins; however, synaptic tau levels were not affected by the absence of parkin (Supplemental File 3). In the hTau/Parkin^{W402A} vs hTau comparison, a total of 262 DEPs were found, 135 upregulated and 127 downregulated

(Fig. 4C). In line with our immunoblotting experiments (Fig. 2), parkin levels were significantly decreased in hTau mice expressing the Parkin^{W402A} mutation (Fig. 4C). Moreover, synaptic tau (Mapt) levels were found to be significantly higher in hTau/Parkin^{W402A}, compared to hTau mice (Fig. 4C).

For further analysis, we first sought to identify the DEPs in hTau vs WT that were also present in the hTau/PKO vs hTau and hTau/Parkin^{W402A} vs hTau comparisons. We found a total of 74 DEPs that were shared across all three comparisons and further categorized them based on general protein function using an artificial intelligence platform (OpenAI. 2025. ChatGPT. <https://www.openai.com/chatgpt>). After confirming the categorization using literature search databases (PubMed and Google Scholar), we generated heatmaps to display each of the shared DEPs under their given category along with their corresponding z-score value (Fig. 5). Interestingly, we found that both the absence of parkin and expression of Parkin^{W402A} predominantly led to opposite effects from what was observed in the hTau vs WT comparison. Only 9 of the 74 shared DEPs between hTau vs WT and hTau/PKO vs hTau showed exacerbating effects, 8 proteins were further downregulated and 1 was further upregulated in the absence of Parkin (Supplemental File 9). For the shared effects between hTau/Parkin^{W402A} vs hTau and hTau vs WT, 4 of the 74 shared DEPs showed exacerbating effects, which were all further downregulated under Parkin^{W402A} (Supplemental File 9).

We next used the STRING database to generate functional protein association networks from our full lists of DEPs. For each comparison (hTau vs WT, hTau/PKO vs hTau, and hTau/Parkin^{W402A} vs hTau) we separately uploaded the significantly upregulated and significantly downregulated proteins and performed the k-means clustering method under a high confidence interaction score (min. Interaction score = 0.7). From the identified clusters (Supplemental File 10), we selected the top upregulated and the top downregulated clusters to discuss. Next, using the GO BP, KEGG, and Reactome databases, we identified the top affected pathways from each of the selected protein clusters based on the given strength score. The strength score represents the ratio between the number of proteins in a given network and the number of proteins expected to be annotated with this term in a random network of the same size.

A total of 18 clusters of DEPs, 12 downregulated and 6 upregulated,

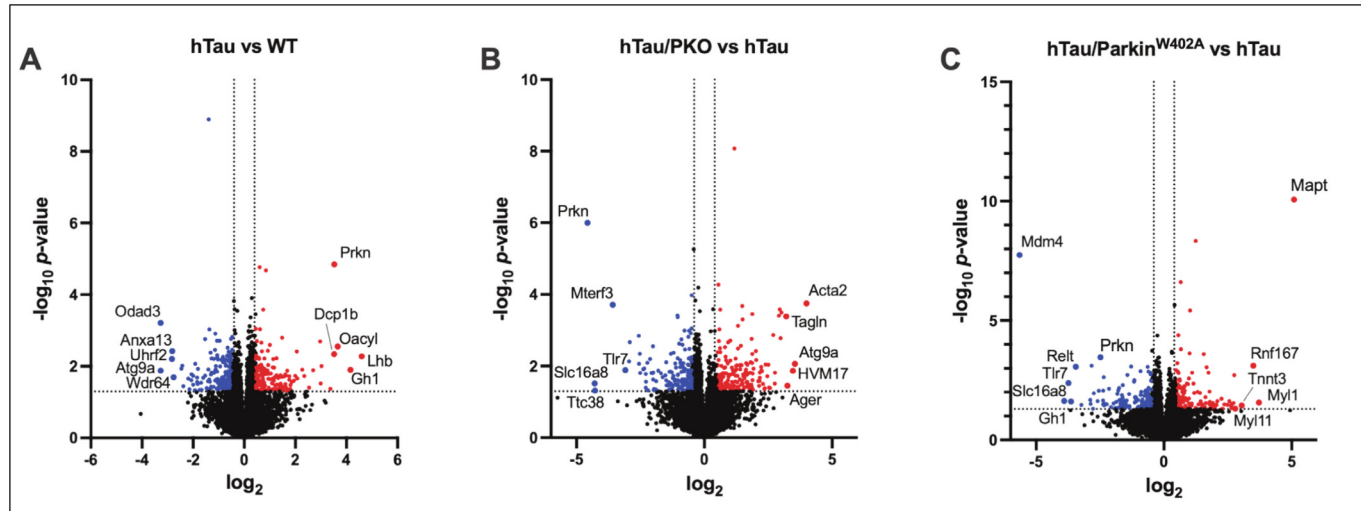


Fig. 4. Identification of differentially expressed proteins (DEPs) in synaptosomes. Volcano plots showing DEPs based on *p*-value obtained from Ms. Stats ($-\log_{10}$) and \log_2 for the 9298 identified proteins. Significance was determined by using *p*-value cutoff = 1.3 (\log_{10}) and z-score cutoff = 1 (absolute value). Blue = significantly downregulated proteins. Red = significantly upregulated proteins. (A) hTau vs WT synaptosome proteomic comparison showed a total of 333 DEPs, 149 upregulated and 184 downregulated. (B) hTau/PKO vs hTau synaptosome proteomic comparison showed a total of 327 DEPs, 179 upregulated and 148 downregulated. (C) hTau/Parkin^{W402A} vs hTau synaptosome proteomic comparison showed a total of 262 DEPs, 135 upregulated and 127 downregulated. *n* = 5 mice per group. The five most highly enriched and depleted proteins are annotated in each comparison. (For interpretation of the references to color in this figure legend, the reader is referred to the web version of this article.)

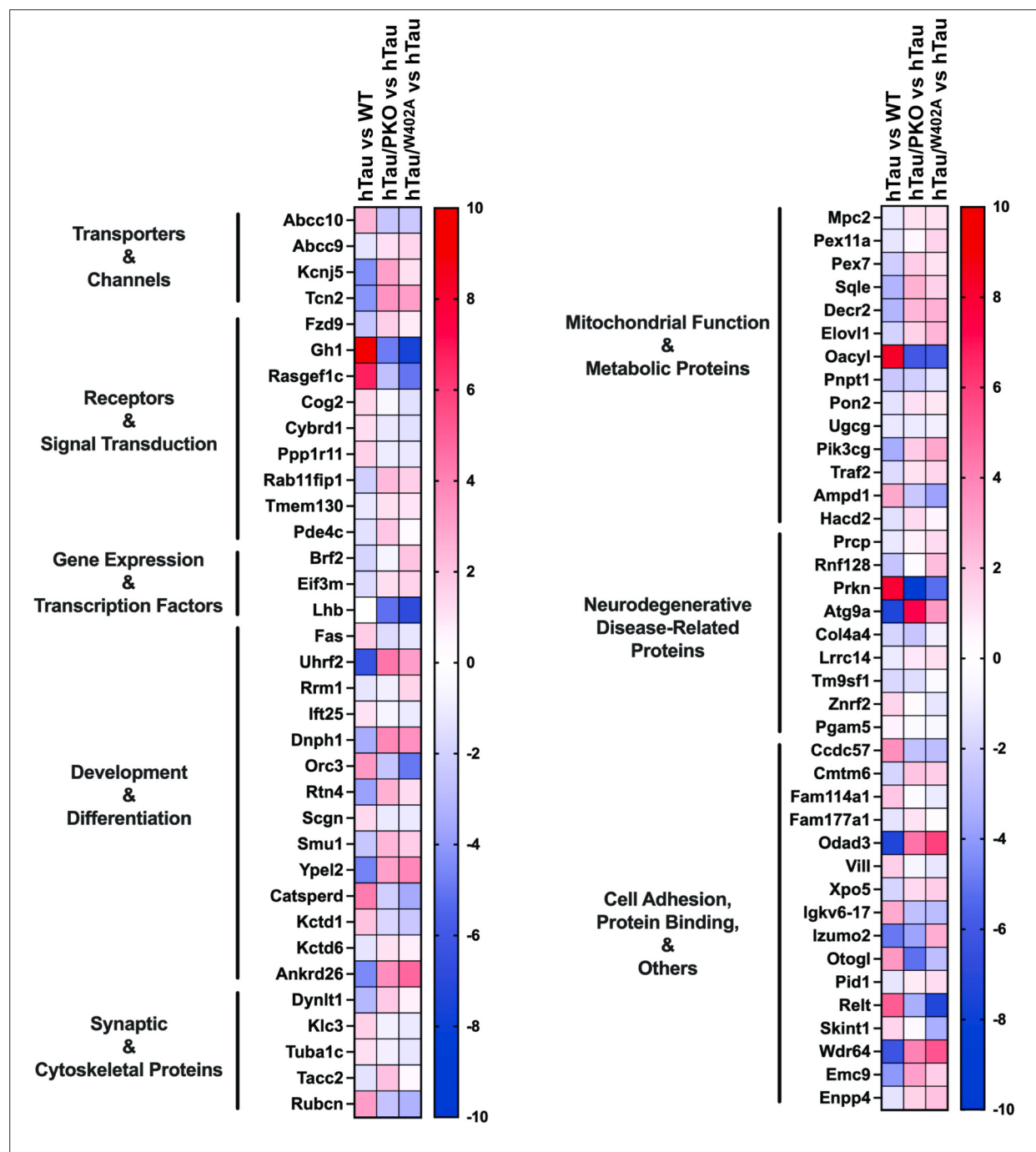


Fig. 5. Analysis of differentially expressed proteins (DEPs) shared between hTau vs WT, hTau/PKO vs hTau, and hTau/Parkin^{W402A} vs hTau. Heatmaps showing the 74 DEPs shared between all the studied comparisons which were identified based on *p*-value obtained from Ms. Stats ($-\log_{10}$) and calculated z-scores (\log_2). Color bar represents each individual z-score. Blue blocks and red blocks represent downregulated and upregulated proteins, respectively. $n = 5$ mice per group. (For interpretation of the references to color in this figure legend, the reader is referred to the web version of this article.)

were identified in the hTau vs WT comparison (**Supplemental File 10**). The top cluster of proteins (Fig. 6A) with the strongest strength score predicted the activation of pathways related to “Neuroactive ligand-receptor interaction” (KEGG ID: mmu04080, strength = 1.61) and “Prolactin receptor signaling” (Reactome ID: MMU-1170546, strength = 2.91) (**Supplemental File 11**), suggesting potential alterations to both neurotransmission and hormone balance. In line with our global GSEA results in Fig. 3C, the cluster of proteins related to the top inactivated pathways (Fig. 6A) was related to “Heparan sulfate proteoglycan biosynthesis” (GO BP ID: 0015012, strength = 2.87),

“Glycosaminoglycan biosynthesis” (KEGG ID: mmu00534, strength = 2.98), and “Heparan sulfate/heparin biosynthesis” (Reactome ID: MMU-1638091, strength = 2.25) (**Supplemental File 11**), reinforcing the synaptic metabolic alterations that may occur in hTau mice, compared to WT mice.

Parkin-null hTau mice displayed a total of 19 clusters of DEPs, 8 downregulated and 11 upregulated, when compared to hTau mice (**Supplemental File 10**). Synaptic protein changes were shown to upregulate protein clusters (Fig. 6B) and predict the activation of pathways involved in “Regulation of membrane repolarization during

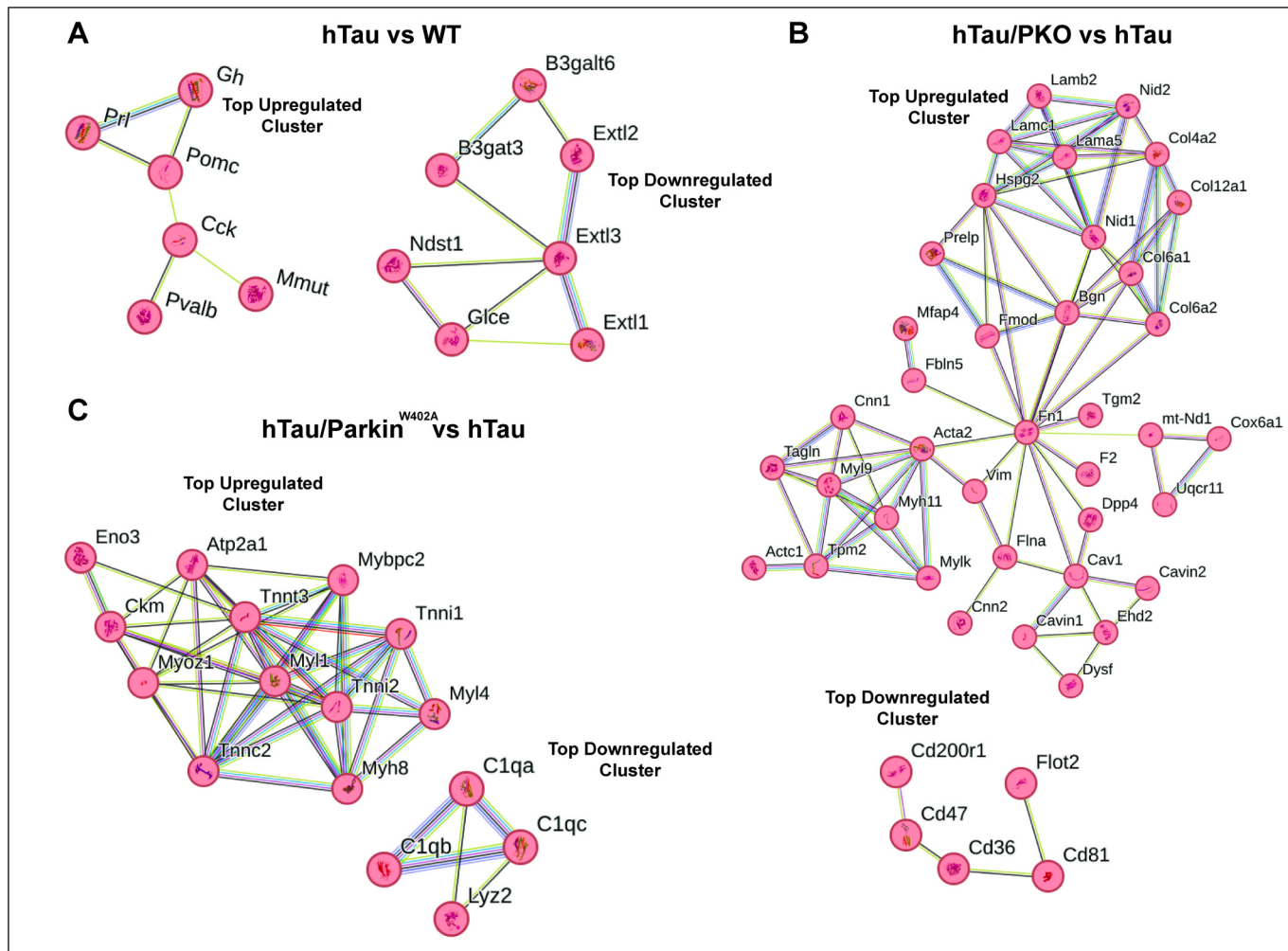


Fig. 6. Analysis of differentially expressed proteins (DEPs) using STRING. The STRING database was used for network analysis of the hTau vs WT, hTau/PKO vs hTau, and hTau/Parkin^{W402A} vs hTau DEPs. The k-means clustering method was used under a high confidence interaction score (min. Interaction score = 0.7). (A) Network representation for the top upregulated and downregulated cluster of proteins in the hTau vs WT comparison. (B) Network representation for the top upregulated and downregulated cluster of proteins in the hTau/PKO vs hTau comparison. (C) Network representation for the top upregulated and downregulated cluster of proteins in the hTau/Parkin^{W402A} vs hTau comparison. $n = 5$ mice per group. The Gene Ontology Biological Process (GO BP), KEGG, and Reactome databases were used to identify changed pathways.

action potentials” (GO BP ID: 0098903, strength = 2.28), “Laminin interactions” (Reactome ID: MMU-3000157, strength = 2.2), “ECM-receptor interaction” (KEGG ID: mmu04512, strength = 1.73), and importantly, coinciding with our results from IPA metabolic pathway analysis (**Fig. 3A**), “Oxidative phosphorylation” (KEGG ID: mmu00190, strength = 1.12) (**Supplemental File 11**). On the other hand, the most downregulated cluster that was identified in hTau/PKO mice (**Fig. 6B**) predicted the inactivation of pathways related to “Cellular responses to low-density lipoprotein” (GO BP ID: 0071404, strength = 2.56) and, contrary to the reported activated pathways, “ECM-receptor interactions” (KEGG ID: 04512, strength = 2.01) also showed a predicted inactivation (**Supplemental File 11**).

In the hTau/Parkin^{W402A} vs hTau comparison, a total of 19 clusters of DEPs, 8 downregulated and 11 upregulated, as observed in the hTau/PKO vs hTau comparison (**Supplemental File 10**). The top upregulated cluster of proteins (**Fig. 6C**) predicted the activation of the “Positive regulation of ATP-dependent activity” (GO BP ID: 0032781, strength = 2.08) and, similar to what we reported in the GSEA global analysis (**Fig. 3E**), “Striated muscle contraction” (Reactome ID: MMU-390522, strength = 2.64) (**Supplemental File 11**). Interestingly, the most downregulated cluster of proteins found in hTau mice under Parkin^{W402A} (**Fig. 6C**) predicted the inhibition of “Synapse pruning” (GO BP

ID: 0098883, strength = 3.21), “Complement system cascade” (KEGG ID: mmu04610, strength = 2.26), and “Classical complement system activation” (Reactome ID: MMU-173623, strength = 3.31) (**Supplemental File 11**).

Here, we identified the DEPs in all of the studied comparisons and used STRING to analyze the predicted changes present in the synaptosomes of hTau mice and the effects that parkin KO and expression of Parkin^{W402A} have on these. We found that several of the previously reported metabolic and neurotransmission-related pathways given by both IPA and GSEA were also found to be affected using STRING. Also, as observed in the GSEA analysis, we found distinct clusters of DEPs in each individual comparison, which predicted distinct affected pathways. Overall, tau accumulation in hTau mice led to changes to the synaptic proteome that predicted alterations to a variety of pathways involved in energy metabolism, synaptic plasticity, and neurotransmission. We also provide evidence that parkin activity can modulate some of these hTau-induced synaptic proteomic changes but can also give rise to other synaptic proteomic alterations that were not previously reported in hTau mice.

3.4. Absence of parkin led to increased levels of pTau in the hippocampal Dentate Gyrus of hTau mice

Increased levels of pTau, particularly in the cortex and hippocampus, are known pathological features of AD (Scheltens et al., 2021). Further, AD-relevant hippocampal tau and pTau accumulation have been previously reported in hTau mice at 8–9 months of age (Andorfer et al., 2003). Here, we aimed to determine whether parkin activity can influence the levels of pTau in hTau mice. For this, we used our generated hTau/PKO and hTau/Parkin^{W402A} mice and compared the levels of hippocampal and cortical pTau to those in hTau mice. To achieve this,

we stained hippocampal sections with antibodies for total tau and pTau (pTauSer202 + pTauT205 using AT8 antibody) and measured the levels of pTau by quantifying the co-localization between total tau and pTau in the DG, pyramidal CA1, pyramidal CA3, and parietal cortex. Our results showed that the absence of Parkin in hTau mice leads to higher levels of tau/AT8 co-localization in the DG (Fig. 7A–B), but not in the CA1 (Supplemental Fig. 6A), CA3 (Supplemental Fig. 6B), nor parietal regions (Fig. 7C–D). In contrast, expression of the Parkin^{W402A} mutation in hTau mice did not affect the levels of pTau in any of the studied regions, when compared to hTau (Fig. 7 and Supplemental Fig. 6).

Our group has recently shown that the number of excitatory synapses

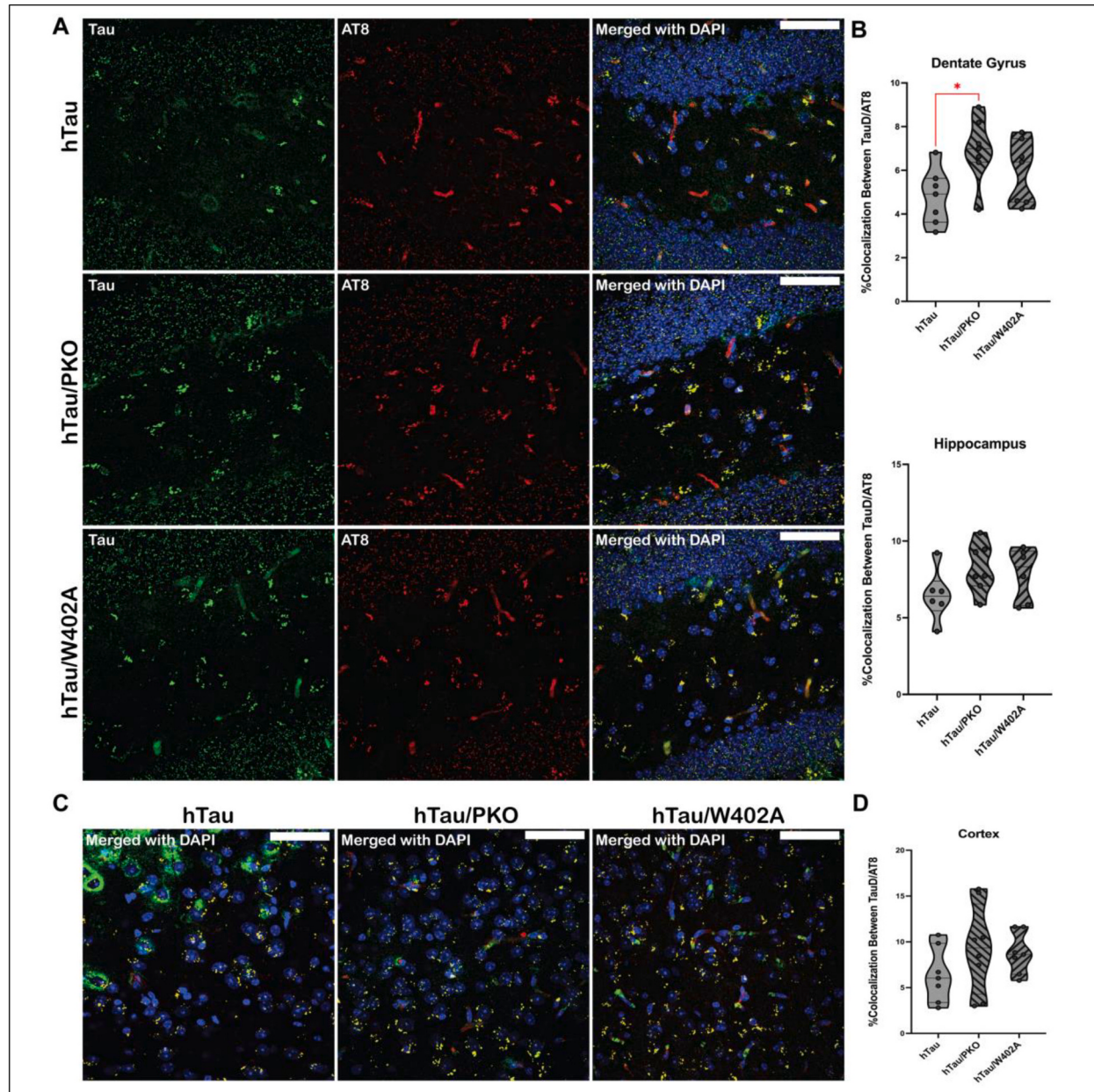


Fig. 7. Absence of Parkin in hTau mice leads to increased pTau in the DG. (A) Representative confocal z-stack images of the DG from 8 to 9-month-old male hTau, hTau/PKO, and hTau/Parkin^{W402A} (hTau/W402A) stained with total Tau (green), AT8 (pTauSer202 + pTauT205, red), and DAPI (blue). Objective = 60×, scale bar = 50 μm. (B) Hippocampal quantifications of the % co-localization between total Tau and AT8 in the DG and the whole hippocampus (integration of DG + CA1 + CA3). (C) Representative confocal z-stack images of the parietal cortex from 8 to 9-month-old male hTau, hTau/PKO, and hTau/Parkin^{W402A} stained with total Tau (green), AT8 (pTauSer202 + pTauT205, red), and DAPI (blue). Objective = 60×, scale bar = 50 μm. (D) Quantification of the % co-localization between total Tau and AT8 in the parietal cortex. Significance: $p < 0.05^*$, one-way ANOVA (DG: genotype DF = 2, and residual DF = 18. Hippocampus: genotype DF = 2, and residual DF = 16. Cortex: genotype DF = 2, and residual DF = 19) followed by Tukey's multiple comparisons test. $n = 6\text{--}8$ mice per group. Violin plot data presented with median and quartiles indicated with dashed lines. DF = degrees of freedom. (For interpretation of the references to color in this figure legend, the reader is referred to the web version of this article.)

in the hippocampus and cortex can be affected by the accumulation of mutant (P301S) human tau (Daniel Estrella et al., 2025). Here, we questioned whether the accumulation of non-mutant human tau can affect the number of excitatory synapses in the hippocampus and/or parietal cortex. To do this, we quantified the number of excitatory synapses within adjacent sections to the pTau staining containing hippocampal and cortical regions by measuring the co-localization between PSD95 (excitatory post-synaptic marker) and synaptophysin (pre-synaptic marker), as previously described (Daniel Estrella et al., 2025). We found no changes in the number of excitatory synapses between hTau and WT mice within the DG (Supplemental Fig. 7), CA1 pyramidal (Supplemental Fig. 8), CA3 pyramidal (Supplemental Fig. 9), and parietal cortex (Supplemental Fig. 10). Additionally, we found that parkin deficiency and expression of Parkin^{W402A} did not alter the number of excitatory synapses in hTau mice.

Altogether, these findings demonstrate that the absence of parkin in hTau mice leads to higher levels of pTau in the hippocampal DG, with no significant changes in the number of excitatory synapses. Expression of Parkin^{W402A} in hTau mice did not alter pTau levels or the number of excitatory synapses. Furthermore, the number of excitatory synapses was unaltered within the studied brain regions in hTau mice at 8–9 months of age.

4. Discussion

Increasing evidence has demonstrated the crucial role that mitochondria play at the synapse, be it through local energy production for proper neurotransmission (Hung et al., 2018; Vos et al., 2010) or to maintain adequate calcium homeostasis (Godoy et al., 2021). Mitochondrial dysfunction, particularly at the synaptic level, is believed to be a key contributor to the cognitive decline and progressive disease alterations that have been observed in both AD patients and preclinical models of AD (Flannagan et al., 2023; Rai et al., 2020; Swerdlow, 2020). In addition to synaptic mitochondrial dysfunction, tau accumulation has been reported at the synapse and shown to enhance pathological tau cell-to-cell propagation (Calafate et al., 2015), alter mitochondrial function (Torres et al., 2021; Trease et al., 2022), and lead to synapse engulfing by reactive microglial cells (Largo-Barrientos et al., 2021; Vogels et al., 2019). We previously reported increased levels of tau (total and hyperphosphorylated) associated with synaptic mitochondria isolated from hTau mice, which coincided with synaptic mitochondrial respiratory dysfunction (Trease et al., 2022). Since parkin plays an important role in maintaining mitochondrial quality, we hypothesized that the loss of parkin would have deleterious consequences on synaptic mitochondrial function, while activating parkin would be protective in hTau mice. Using novel hTau/PKO mice generated herein, we found that the absence of parkin in hTau mice leads to mitochondrial respiratory dysfunction in synaptosomes. Interestingly, Damiano et al. showed that parkin-deficient mice had reduced mitochondrial respiration in striatal neurons, but not in cortical neurons (Damiano et al., 2014).

In contrast to our hypothesis, expressing Parkin^{W402A} did not alter synaptic mitochondrial respiratory function in hTau mice. Previous studies looking at different mutant forms of parkin have characterized some of the genetic alterations that lead to activation or inactivation of parkin activity (Sauve et al., 2022; Tang et al., 2017; Trempe et al., 2013). For instance, Tang et al. identified some of these parkin-activating mutations, like the Parkin^{F146A} (within the RING0 domain) and the Parkin^{W403A} (within the REP domain) mutations (Tang et al., 2017). For the Parkin^{W403A} mutation in particular, Trempe et al. and Sauvé et al. provided *in vitro* evidence that Parkin^{W403A} (human correlate of the mouse Parkin^{W402A} mutation) leads to higher parkin activity and recruitment to the mitochondria, highlighting its potential therapeutic benefits for rescuing mitochondrial quality control in disease state (Sauvé et al., 2022; Trempe et al., 2013). However, to the best of our knowledge, no evidence has been shown regarding the *in vivo* effects that human Parkin^{W403A} has on parkin's activity within the brain.

Here, we used Parkin^{W402A}, the murine correlate of human Parkin^{W403A}, to test the hypothesis that enhanced parkin activity in hTau mice would rescue the effects that were observed in hTau mice. Overall, the Parkin^{W402A} mutation does not seem to rescue synaptic mitochondrial function nor the levels of pTau in hTau mice. In fact, our immunoblotting data shows that Parkin^{W402A} mutation leads to lower levels of the parkin protein. It is important to note that our data does not directly contradict the findings suggesting that the Parkin^{W402A} mutation may still lead to increased parkin activation; in fact, our findings suggest that the Parkin^{W402A} mutation – be it due to a chronic protein activation or other unknown pathways – triggers the *in vivo* downregulation and/or the turnover of parkin, decreasing its overall protein levels.

Our findings that genetic ablation of parkin exacerbates synaptic mitochondrial respiratory function impairments in hTau mice reveals that parkin is important in mitochondrial quality control in the hTau mouse model. Here, we also provide *in vivo* evidence of parkin recruitment to the synaptic mitochondria of hTau mice, suggesting increased mitophagy. Importantly, our immunoblots showed that the levels of parkin within the brain homogenate of hTau mice were significantly reduced, compared to WT. Interestingly, studies in both preclinical models of AD and *post-mortem* human tissue from AD patients have predominantly reported a significant decrease in the levels of parkin within the brain (Braun and Pugliali, 2022; Fang et al., 2019; Khandelwal et al., 2011; Martin-Maestro et al., 2016). For instance, Martín-Maestro et al. showed decreased levels of parkin in *post-mortem* fibroblast samples from sporadic AD patients (Martin-Maestro et al., 2016). Furthermore, Ye et al. showed a progressive reduction in the levels of Parkin within cortical *post-mortem* brain samples from AD patients during different stages of disease (Ye et al., 2015). Nevertheless, Ye et al. also reported that, in isolated mitochondrial fractions from the brains of AD patients, the levels of parkin were significantly elevated, suggesting an enhanced parkin translocation to defective mitochondria that, upon constant lysosomal degradation, reflects an overall reduction in the levels of parkin within the brain (Ye et al., 2015). Our data shown here further expand on the findings presented by Ye et al. by providing evidence of increased parkin translocation to synaptic mitochondrial fractions and detection of elevated mitochondrial ubiquitination in a mouse model that shows AD-relevant tau pathology (hTau mice), highlighting the fact that induction of mitophagy could also take place in the absence of amyloid beta pathology. Parkin deficiency in hTau mice led to reduced synaptic mitochondrial ubiquitination revealing that parkin is mediating this. Additionally, our brain homogenate samples also showed a decrease in the levels of parkin in hTau mice, similarly to the findings from Ye et al. using brain samples from AD patients, further validating the use of the hTau mouse model for studying AD-related pathophysiology. While we found increased parkin translocation to synaptic mitochondria in hTau mice, previous studies in neuroblastoma cells found that tau (both human WT and mutant P301L) inhibits mitophagy by interacting with parkin in the cytosol and reducing parkin translocation to mitochondria (Cummins et al., 2019), thus future studies could interrogate whether parkin and tau interact in the mouse brain. Despite the observed changes in parkin, we did not uncover evidence for changes in mitochondrial mass nor autophagosome formation; however, we note that autophagy/mitophagy are dynamic processes and biochemical analysis is only assessing static measures and not flux.

Our proteomic analyses demonstrated significant changes in the abundance levels of synaptosomal proteins in hTau mice, which upon functional annotation, predicted changes to numerous metabolic and signaling pathways. The metabolic pathways that were most affected by all three manipulations (hTau vs WT, hTau/PKO vs hTau, and hTau/Parkin^{W402A} vs hTau) were predominantly those related to mitochondrial homeostasis and energy metabolism. In particular, the predicted activation of oxidative phosphorylation, shown in both our IPA and GSEA analyses, provides evidence of potential compensatory mechanisms to maintain synaptic mitochondrial respiratory function, as hTau mice exhibit impaired synaptic mitochondrial respiratory dysfunction

(Trease et al., 2022). Furthermore, inactivation of phosphatidylglycerol biosynthesis in hTau vs WT mice, highlighted in both IPA and GSEA analyses, could lead to a downstream reduction in the levels of cardiolipin, which maintain inner mitochondrial membrane potential and membrane structure, potentially contributing to the observed synaptic mitochondrial respiratory alterations. Indeed, a previous study by Monteiro-Cardoso et al. showed that reduced levels of cardiolipin in a murine model of AD correlate with observed synaptic mitochondrial bioenergetic failure (Monteiro-Cardoso et al., 2015). Interestingly, while the absence of parkin in hTau mice exacerbated the synaptic mitochondrial respiratory impairment observed in hTau mice, the phosphatidylglycerol biosynthesis pathway remained unchanged. However, it is important to mention that other metabolic pathways involved in mitochondrial homeostasis, like oxidative phosphorylation and ketolysis, were affected by the absence of parkin in hTau mice, which could have contributed to the synaptic bioenergetic failure. The expression of Parkin^{W402A} in hTau mice did indeed rescue phosphatidylglycerol biosynthesis by predicting its activation, but these Parkin^{W402A}-induced rescuing effects were not able to modulate the synaptic mitochondrial respiratory alterations that were previously observed in hTau mice. We previously studied the synaptic mitochondrial proteome alterations in hTau vs WT mice (Trease et al., 2022) and note that several metabolic pathways predicted to be activated and/or inhibited showed opposite predictions based on the synaptosomal proteomics presented here, which is likely due to the contribution of cytosolic proteins to these metabolic pathways that were missing in our previous dataset; however, the methods used for mass spectrometry between these two studies were different (SCIEX TTOF 5600 SWATH-MS on synaptic mitochondria vs Thermo Orbitrap Fusion Lumos Tribrid Spectronaut directDIA), limiting direct data comparison.

Synaptic plasticity pathways, such as long-term potentiation (LTP) and long-term depression (LTD), remain essential mechanisms for proper brain functioning and cognitive performance (Lu et al., 2014; Zheng et al., 2022). In line with our proteomic results, in which LTP and LTD were predicted to be inactivated in the synaptosomes of hTau mice, similar reports using functional approaches have shown that LTP and overall synaptic plasticity are diminished in both hTau mice and other AD-related models (Fa et al., 2016; Polydoro et al., 2009; Shentu et al., 2018). Notably, both the absence of parkin and expression of Parkin^{W402A} in hTau mice appear to exacerbate these hTau-induced synaptic plasticity alterations, reflected by further predicted inactivation of synaptic plasticity-related pathways like LTP, LTD, and CREB-signaling. These results demonstrate that the protective effects of parkin go beyond mitochondrial-related pathways and are able to influence hTau-induced alterations to neuronal plasticity and neurotransmission. Interestingly, Parkin^{W402A} in hTau mice led to a drastic increase in the levels of tau at the synapse, suggesting that this modulation may exacerbate the aberrant hTau-induced tau accumulation, rather than reverse it. While Parkin^{W402A} in hTau mice had effects to the synaptic proteome that were similar to those observed under the absence of parkin in hTau mice, certain pathways did appear to be Parkin^{W402A}-specific. The latter calls for further in-depth investigations on the effect that this mutation has on parkin and the role it plays under tau accumulation.

Pathological alterations in hTau mice have been previously described within the hippocampus and neocortex (Andorfer et al., 2003). Also, Polydoro et al. showed accumulation of different pTau forms in the hippocampal CA1/CA3 pyramidal cell layers along with synaptic plasticity alterations in hTau mice (Polydoro et al., 2009). More specifically, Menéndez et al. developed a mouse model of fronto-temporal dementia with parkinsonism linked to chromosome 17 (FTDP-17) under the absence of parkin, which exhibited both exacerbated nigrostriatal alterations and tau accumulation, further highlighting the role of parkin in FTDP-17 (Menéndez et al., 2006). In the present study, we questioned whether the absence of parkin in hTau mice would further exacerbate the hTau-induced accumulation of pTau in the hippocampus. We found increased levels of pTau in the DG of parkin-null

hTau mice, when compared to hTau mice, while the pyramidal cell layers of the CA1 and CA3 remained spared. Using the mouse model generated in Menéndez et al., and in line with our results reported here, Rodríguez-Navarro et al. showed that the absence of parkin in Tau^{VLW} mice (PK^{-/-}/Tau^{VLW}) led to increased pTau staining in the hippocampus, including the DG (Menéndez et al., 2006; Rodríguez-Navarro et al., 2008). Importantly, the changes to tau levels in the hippocampus of PK^{-/-}/Tau^{VLW} mice shown by Rodríguez-Navarro et al. were more prominent than those reported in our study (Rodríguez-Navarro et al., 2008; Rodríguez-Navarro et al., 2010). However, it is important to note that the PK^{-/-}/Tau^{VLW} model could be considered to have a more aggressive form of tau pathology, as it uses an overexpression of human mutant tau (human four-repeat tau isoform with two N-terminal exons carrying the mutations G272V, P301L and R406W) (Menéndez et al., 2006), whereas the present study uses a non-mutant overexpression of all six isoforms of human tau (Andorfer et al., 2003) under the absence of parkin.

Importantly, some limitations to our study can be identified. For instance, sex as a biological variable has been recognized to be an important factor when making population assumptions based on experimental results. In this study, only male mice were utilized for experimentation. Future research will uncover whether female mice exhibit similar or distinct changes as compared to male mice. The use of tissue fractionations from the whole fore/hindbrain (excluding the cerebellum and olfactory bulbs), rather than AD-relevant regions that have shown to exhibit tau pathology (i.e., hippocampus and neocortex), potentially dilutes the degree of significance in some of our findings. Future studies should focus on synaptosomes isolated from such brain regions.

5. Conclusions

The present study investigated the influence that modulating parkin in hTau mice has on synaptic mitochondrial respiratory dysfunction and on the synaptic proteome, testing the hypothesis that parkin deficiency will have deleterious consequences, while expressing Parkin^{W402A} may be protective. For this, we developed two novel mouse models by crossing hTau mice (express all six nonmutant human tau isoforms in the absence of murine Tau) with parkin knockout mice (hTau/PKO) and mice with a predicted overactive mutant form of parkin (hTau/Parkin^{W402A}). Here, we show that parkin deficiency leads to mitochondrial respiratory and glycolytic dysfunction in synaptosomes from hTau mice. Further, we report for the first time that hTau mice display synaptic proteomic alterations, predominantly to pathways related to mitochondrial metabolism, synaptic long-term potentiation, synaptic calcium homeostasis, and other relevant metabolic and signaling pathways. Both the absence of parkin and expression of Parkin^{W402A} led to further changes in the hTau mouse synaptic proteome, particularly to those related to mitochondrial metabolism and synaptic plasticity. We also provide evidence of significant parkin translocation to synaptic mitochondria isolated from hTau mice that coincides with increased mitochondrial ubiquitination, suggesting increased mitophagy at the synapse. Our data also showed that parkin levels have an effect on the levels of pTau, as parkin-null hTau mice showed increased pTau in the hippocampal DG, compared to hTau. In conclusion, this research illustrates the protective role of parkin against hTau-induced synaptic mitochondrial dysfunction and tau accumulation. Our findings emphasize the protective effects that parkin activity has against tau-induced mitochondrial dysfunction and other tau-induced synaptic alterations that are also observed in different tauopathies, like AD.

Supplementary data to this article can be found online at <https://doi.org/10.1016/j.nbd.2025.107084>.

Funding and acknowledgements

This work was supported by the National Institutes of Health and

National Institutes of Aging grant R01AG059785. The authors thank Dr. Howard Fox for invaluable scientific input. Mass spectrometry analyses were performed by the University of Nebraska Medical Center Multiomics Mass Spectrometry Core Facility (RRID: SCR_012539).

Declaration of generative AI and AI-assisted technologies in the analysis process

During the analysis of this work, particularly in the proteomics data, the authors used *ChatGPT* in order to categorize shared differentially expressed proteins based on general protein function. After using this tool/service, the authors reviewed and edited the content as needed and take full responsibility for the content of the published article.

CRediT authorship contribution statement

L. Daniel Estrella: Writing – review & editing, Writing – original draft, Visualization, Validation, Supervision, Project administration, Methodology, Investigation, Formal analysis, Data curation, Conceptualization. **Xiaoke Xu:** Writing – review & editing, Writing – original draft, Methodology, Investigation, Formal analysis, Data curation. **Collin White:** Writing – review & editing, Formal analysis, Data curation. **Jane E. Manganaro:** Writing – review & editing, Project administration, Data curation. **Lexi Sheldon:** Writing – review & editing, Project administration. **Trey Farmer:** Project administration, Conceptualization. **Kelly L. Stauch:** Writing – review & editing, Writing – original draft, Visualization, Supervision, Resources, Project administration, Investigation, Funding acquisition, Conceptualization.

Declaration of competing interest

The authors declare that they have no known competing financial interests or personal relationships that could have appeared to influence the work reported in this manuscript.

Data availability

Data will be made available on request.

References

- Andorfer, C., Kress, Y., Espinoza, M., de Silva, R., Tucker, K.L., Barde, Y.A., Duff, K., Davies, P., 2003. Hyperphosphorylation and aggregation of tau in mice expressing normal human tau isoforms. *J. Neurochem.* 86 (3), 582–590.
- Ashrafi, G., Schlehe, J.S., LaVoie, M.J., Schwarz, T.L., 2014. Mitophagy of damaged mitochondria occurs locally in distal neuronal axons and requires PINK1 and Parkin. *J. Cell Biol.* 206 (5), 655–670.
- Birdsall, V., Waites, C.L., 2019. Autophagy at the synapse. *Neurosci. Lett.* 697, 24–28.
- Braun, M.M., Puglisi, L., 2022. Defective PTEN-induced kinase 1/Parkin mediated mitophagy and neurodegenerative diseases. *Front. Cell. Neurosci.* 16, 1031153.
- Calafate, S., Buijs, A., Miskiewicz, K., Vijayan, V., Daneels, G., de Strooper, B., de Wit, J., Verstreken, P., Moearchs, D., 2015. Synaptic contacts enhance cell-to-cell tau pathology propagation. *Cell Rep.* 11 (8), 1176–1183.
- Chen, Z., Chen, B., Xu, W.F., Liu, R.F., Yang, J., Yu, C.X., 2012. Effects of PTEN inhibition on regulation of tau phosphorylation in an okadaic acid-induced neurodegeneration model. *Int. J. Dev. Neurosci.* 30 (6), 411–419.
- Chen, Y., Fu, A.K.Y., Ip, N.Y., 2019. Synaptic dysfunction in Alzheimer's disease: mechanisms and therapeutic strategies. *Pharmacol. Ther.* 195, 186–198.
- Choi, S.W., Gerencser, A.A., Nicholls, D.G., 2009. Bioenergetic analysis of isolated cerebrocortical nerve terminals on a microgram scale: spare respiratory capacity and stochastic mitochondrial failure. *J. Neurochem.* 109 (4), 1179–1191.
- Cummins, N., Tweedie, A., Zuryan, S., Bertran-Gonzalez, J., Gotz, J., 2019. Disease-associated tau impairs mitophagy by inhibiting Parkin translocation to mitochondria. *EMBO J.* 38 (3).
- Damiano, M., Gautier, C.A., Bulteau, A.L., Ferrando-Miguel, R., Gourane, C., Paoli, M.G., Pruss, R., Auchere, F., L'Hermitte-Stead, C., Bouillaud, F., Brice, A., Corti, O., Lombes, A., 2014. Tissue- and cell-specific mitochondrial defect in Parkin-deficient mice. *PLoS One* 9 (6), e99898.
- Daniel Estrella, L., Trease, A.J., Sheldon, L., Roland, N.J., Fox, H.S., Stauch, K.L., 2025. Tau association with synaptic mitochondria coincides with energetic dysfunction and excitatory synapse loss in the P301S tauopathy mouse model. *Neurobiol. Aging* 147, 163–175.
- Du, H., Guo, L., Fang, F., Chen, D., Sosunov, A.A., McKhann, G.M., Yan, Y., Wang, C., Zhang, H., Molkentin, J.D., Gunn-Moore, F.J., Vonsattel, J.P., Arancio, O., Chen, J.X., Yan, S.D., 2008. Cyclophilin D deficiency attenuates mitochondrial and neuronal perturbation and ameliorates learning and memory in Alzheimer's disease. *Nat. Med.* 14 (10), 1097–1105.
- Duarte, F.V., Ciampi, D., Duarte, C.B., 2023. Mitochondria as central hubs in synaptic modulation. *Cell. Mol. Life Sci.* 80 (6), 173.
- Fa, M., Puzzo, D., Piacentini, R., Staniszewski, A., Zhang, H., Baltrons, M.A., Li Puma, D. D., Chatterjee, I., Li, J., Saeed, F., Berman, H.L., Ripoli, C., Gulisano, W., Gonzalez, J., Tian, H., Costa, J.A., Lopez, P., Davidowitz, E., Yu, W.H., Haroutunian, V., Brown, L.M., Palmeri, A., Sigurdsson, E.M., Duff, K.E., Teich, A.F., Honig, L.S., Siersk, M., Moe, J.G., D'Adamo, L., Grassi, C., Kanaan, N.M., Fraser, P. E., Arancio, O., 2016. Extracellular tau oligomers produce an immediate impairment of LTP and memory. *Sci. Rep.* 6, 19393.
- Fang, E.F., Hou, Y., Palikaras, K., Adriaanse, B.A., Kerr, J.S., Yang, B., Lautrup, S., Hasan-Olive, M.M., Capanio, D., Dan, X., Rocktaschel, P., Croteau, D.L., Akbari, M., Greig, N.H., Fladby, T., Nilsen, H., Cader, M.Z., Mattson, M.P., Tavernarakis, N., Bohr, V.A., 2019. Mitophagy inhibits amyloid-beta and tau pathology and reverses cognitive deficits in models of Alzheimer's disease. *Nat. Neurosci.* 22 (3), 401–412.
- Flanagan, K., Stopperan, J.A., Hauger, B.M., Troutwine, B.R., Lysaker, C.R., Strope, T. A., Csikos Drummond, V., Gilmore, C.A., Swerdlow, N.A., Draper, J.M., Gouvion, C. M., Vivian, J.L., Haeri, M., Swerdlow, R.H., Wilkins, H.M., 2023. Cell type and sex specific mitochondrial phenotypes in iPSC derived models of Alzheimer's disease. *Front. Mol. Neurosci.* 16, 1201015.
- Godoy, J.A., Rios, J.A., Picon-Pages, P., Herrera-Fernandez, V., Swaby, B., Crepin, G., Vicente, R., Fernandez-Fernandez, J.M., Munoz, F.J., 2021. Mitostasis, calcium and free radicals in health, aging and neurodegeneration. *Biomolecules* 11 (7).
- Goldberg, M.S., Fleming, S.M., Palacino, J.J., Cepeda, C., Lam, H.A., Bhatnagar, A., Meloni, E.G., Wu, N., Ackerson, L.C., Klapstein, G.J., Gajendiran, M., Roth, B.L., Chesselet, M.F., Maidment, N.T., Levine, M.S., Shen, J., 2003. Parkin-deficient mice exhibit nigrostriatal deficits but not loss of dopaminergic neurons. *J. Biol. Chem.* 278 (44), 43628–43635.
- Gupta, A., Dey, C.S., 2012. PTEN, a widely known negative regulator of insulin/PI3K signaling, positively regulates neuronal insulin resistance. *Mol. Biol. Cell* 23 (19), 3882–3898.
- Henrique, A.M., Gianetti, N.G., Ferrari, M.F.R., 2021. Parkin is downregulated among autophagy-related proteins prior to hyperphosphorylation of tau in TS65DN mice. *Biochem. Biophys. Res. Commun.* 561, 59–64.
- Hesse, R., Hurtado, M.L., Jackson, R.J., Eaton, S.L., Herrmann, A.G., Colom-Cadena, M., Tzioras, M., King, D., Rose, J., Tulloch, J., McKenzie, C.A., Smith, C., Henridge, C. M., Lamont, D., Wishart, T.M., Spires-Jones, T.L., 2019. Comparative profiling of the synaptic proteome from Alzheimer's disease patients with focus on the APOE genotype. *Acta Neuropathol. Commun.* 7 (1), 214.
- Hu, Y., Li, X.C., Wang, Z.H., Luo, Y., Zhang, X., Liu, X.P., Feng, Q., Wang, Q., Yue, Z., Chen, Z., Ye, K., Wang, J.Z., Liu, G.P., 2016. Tau accumulation impairs mitophagy via increasing mitochondrial membrane potential and reducing mitochondrial Parkin. *Oncotarget* 7 (14), 17356–17368.
- Hung, C.H., Cheng, S.S., Cheung, Y.T., Wuwongse, S., Zhang, N.Q., Ho, Y.S., Lee, S.M., Chang, R.C., 2018. A reciprocal relationship between reactive oxygen species and mitochondrial dynamics in neurodegeneration. *Redox Biol.* 14, 7–19.
- Khandelwal, P.J., Herman, A.M., Hoe, H.S., Rebeck, G.W., Moussa, C.E., 2011. Parkin mediates beclin-dependent autophagic clearance of defective mitochondria and ubiquitinated Abeta in AD models. *Hum. Mol. Genet.* 20 (11), 2091–2102.
- Kim, M., Nikouee, A., Sun, Y., Zhang, Q.J., Liu, Z.P., Zang, Q.S., 2022. Evaluation of Parkin in the regulation of myocardial mitochondria-associated membranes and cardiomyopathy during Endotoxemia. *Front. Cell Dev. Biol.* 10, 796061.
- Koffie, R.M., Hyman, B.T., Spires-Jones, T.L., 2011. Alzheimer's disease: synapses gone cold. *Mol. Neurodegener.* 6 (1), 63.
- Lamberty, B.G., Estrella, L.D., Mattingly, J.E., Emanuel, K., Trease, A., Totusek, S., Sheldon, L., George, J.W., Almkhlaifi, M.A., Farmer, T., Stauch, K.L., 2023. Parkinson's disease relevant pathological features are manifested in male Pink1/Parkin deficient rats. *Brain Behav Immun Health* 31, 100656.
- Lane, C.A., Hardy, J., Schott, J.M., 2018. Alzheimer's disease. *Eur. J. Neurol.* 25 (1), 59–70.
- Largo-Barrientos, P., Apostolo, N., Creemers, E., Callaerts-Vegh, Z., Swerts, J., Davies, C., McInnes, J., Wierda, K., De Strooper, B., Spires-Jones, T., de Wit, J., Utterhoeven, V., Verstreken, P., 2021. Lowering Synaptogyrin-3 expression rescues Tau-induced memory defects and synaptic loss in the presence of microglial activation. *Neuron* 109 (5), 767–777 e765.
- Lecca, D., Jung, Y.J., Scerba, M.T., Hwang, I., Kim, Y.K., Kim, S., Modrow, S., Tweedie, D., Hsueh, S.C., Liu, D., Luo, W., Glotfelty, E., Li, Y., Wang, J.Y., Luo, Y., Hoffer, B.J., Kim, D.S., McDevitt, R.A., Greig, N.H., 2022. Role of chronic neuroinflammation in neuroplasticity and cognitive function: a hypothesis. *Alzheimers Dement.* 18 (11), 2327–2340.
- Li, S., Sheng, Z.H., 2022. Energy matters: presynaptic metabolism and the maintenance of synaptic transmission. *Nat. Rev. Neurosci.* 23 (1), 4–22.
- Lichter, E.Z., Trease, A.J., Cooper, K., Stauch, K.L., Fox, H.S., 2023. Effects of Parkin on the mitochondrial genome in the heart and brain of mitochondrial Mutator mice. *Adv Biol (Weinh)* 7 (8), e2300154.
- Liu-Yesuevitz, L., Bassell, G.J., Gitler, A.D., Hart, A.C., Klann, E., Richter, J.D., Warren, S.T., Wolozin, B., 2011. Local RNA translation at the synapse and in disease. *J. Neurosci.* 31 (45), 16086–16093.
- Lu, B., Nagappan, G., Lu, Y., 2014. BDNF and synaptic plasticity, cognitive function, and dysfunction. *Handb. Exp. Pharmacol.* 220, 223–250.

- Martin-Maestro, P., Gargini, R., Perry, G., Avila, J., Garcia-Escudero, V., 2016. PARK2 enhancement is able to compensate mitophagy alterations found in sporadic Alzheimer's disease. *Hum. Mol. Genet.* 25 (4), 792–806.
- Menendez, J., Rodriguez-Navarro, J.A., Solano, R.M., Casarejos, M.J., Rodal, I., Guerrero, R., Sanchez, M.P., Avila, J., Mena, M.A., de Yebenes, J.G., 2006. Suppression of Parkin enhances nigrostriatal and motor neuron lesion in mice over-expressing human-mutated tau protein. *Hum. Mol. Genet.* 15 (13), 2045–2058.
- Monteiro-Cordoso, V.F., Oliveira, M.M., Melo, T., Domingues, M.R., Moreira, P.I., Ferreiro, E., Peixoto, F., Videira, R.A., 2015. Cardiolipin profile changes are associated to the early synaptic mitochondrial dysfunction in Alzheimer's disease. *J Alzheimer's Dis* 43 (4), 1375–1392.
- Narendra, D.P., Youle, R.J., 2024. The role of PINK1-Parkin in mitochondrial quality control. *Nat. Cell Biol.* 26 (10), 1639–1651.
- Ordureau, A., Paulo, J.A., Zhang, W., Ahfeldt, T., Zhang, J., Cohn, E.F., Hou, Z., Heo, J. M., Rubin, L.L., Sidhu, S.S., Gygi, S.P., Harper, J.W., 2018. Dynamics of PARKIN-dependent mitochondrial ubiquitylation in induced neurons and model systems revealed by digital snapshot proteomics. *Mol. Cell* 70 (2), 211–227 e218.
- Pickett, E.K., Rose, J., McCrory, C., McKenzie, C.A., King, D., Smith, C., Gillingwater, T. H., Henridge, C.M., Spires-Jones, T.L., 2018. Region-specific depletion of synaptic mitochondria in the brains of patients with Alzheimer's disease. *Acta Neuropathol.* 136 (5), 747–757.
- Polydoro, M., Acker, C.M., Duff, K., Castillo, P.E., Davies, P., 2009. Age-dependent impairment of cognitive and synaptic function in the tau mouse model of tau pathology. *J. Neurosci.* 29 (34), 10741–10749.
- Rai, S.N., Singh, C., Singh, A., Singh, M.P., Singh, B.K., 2020. Mitochondrial dysfunction: a potential therapeutic target to treat Alzheimer's disease. *Mol. Neurobiol.* 57 (7), 3075–3088.
- Randez-Gil, F., Bojunga, L., Estruch, F., Winderickx, J., Del Poeta, M., Prieto, J.A., 2020. Sphingolipids and inositol phosphates regulate the tau protein phosphorylation status in humanized yeast. *Front. Cell Dev. Biol.* 8, 592159.
- Rodriguez-Navarro, J.A., Gomez, A., Rodal, I., Perucho, J., Martinez, A., Furio, V., Ampuero, I., Casarejos, M.J., Solano, R.M., de Yebenes, J.G., Mena, M.A., 2008. Parkin deletion causes cerebral and systemic amyloidosis in human mutated tau over-expressing mice. *Hum. Mol. Genet.* 17 (20), 3128–3143.
- Rodriguez-Navarro, J.A., Rodriguez, L., Casarejos, M.J., Solano, R.M., Gomez, A., Perucho, J., Cuervo, A.M., Garcia de Yebenes, J., Mena, M.A., 2010. Trehalose ameliorates dopaminergic and tau pathology in parkin deleted/tau overexpressing mice through autophagy activation. *Neurobiol. Dis.* 39 (3), 423–438.
- Samanta, S., Akhter, F., Roy, A., Chen, D., Turner, B., Wang, Y., Clemente, N., Wang, C., Swerdlow, R.H., Battaile, K.P., Lovell, S., Yan, S.F., Yan, S.S., 2024. New cyclophilin D inhibitor rescues mitochondrial and cognitive function in Alzheimer's disease. *Brain* 147 (5), 1710–1725.
- Saura, C.A., Valero, J., 2011. The role of CREB signaling in Alzheimer's disease and other cognitive disorders. *Rev. Neurosci.* 22 (2), 153–169.
- Sauve, V., Sung, G., MacDougall, E.J., Kozlov, G., Saran, A., Fakih, R., Fon, E.A., Gehring, K., 2022. Structural basis for feedforward control in the PINK1/Parkin pathway. *EMBO J.* 41 (12), e109460.
- Scheltens, P., De Strooper, B., Kirvelo, M., Holstege, H., Chetelat, G., Teunissen, C.E., Cummings, J., van der Flier, W.M., 2021. Alzheimer's disease. *Lancet* 397 (10284), 1577–1590.
- Schindelin, J., Arganda-Carreras, I., Frise, E., Kaynig, V., Longair, M., Pietzsch, T., Preibisch, S., Rueden, C., Saalfeld, S., Schmid, B., Tinevez, J.Y., White, D.J., Hartenstein, V., Eliceiri, K., Tomancak, P., Cardona, A., 2012. Fiji: an open-source platform for biological-image analysis. *Nat. Methods* 9 (7), 676–682.
- Scholl, M., Lockhart, S.N., Schonhaut, D.R., O'Neil, J.P., Janabi, M., Oszenkoppele, R., Baker, S.L., Vogel, J.W., Faria, J., Schwimmer, H.D., Rabinovici, G.D., Jagust, W.J., 2016. PET imaging of tau deposition in the aging human brain. *Neuron* 89 (5), 971–982.
- Shentu, Y.P., Huo, Y., Feng, X.L., Gilbert, J., Zhang, Q., Liuyang, Z.Y., Wang, X.L., Wang, G., Zhou, H., Wang, X.C., Wang, J.Z., Lu, Y.M., Westermark, J., Man, H.Y., Liu, R., 2018. CIP2A causes tau/APP phosphorylation, Synaptopathy, and memory deficits in Alzheimer's disease. *Cell Rep.* 24 (3), 713–723.
- Shimohama, S., Tanino, H., Sumida, Y., Tsuda, J., Fujimoto, S., 1998. Alteration of myoinositol monophosphatase in Alzheimer's disease brains. *Neurosci. Lett.* 245 (3), 159–162.
- Snel, B., Lehmann, G., Bork, P., Huynen, M.A., 2000. STRING: a web-server to retrieve and display the repeatedly occurring neighbourhood of a gene. *Nucleic Acids Res.* 28 (18), 3442–3444.
- Stevens, M.U., Croteau, N., Eldeeb, M.A., Antico, O., Zeng, Z.W., Toth, R., Durcan, T.M., Springer, W., Fon, E.A., Muqit, M.M., Trempe, J.F., 2023. Structure-based design and characterization of Parkin-activating mutations. *Life Sci Alliance* 6 (6).
- Subramanian, A., Tamayo, P., Mootha, V.K., Mukherjee, S., Ebert, B.L., Gillette, M.A., Paulovich, A., Pomeroy, S.L., Golub, T.R., Lander, E.S., Mesirov, J.P., 2005. Gene set enrichment analysis: a knowledge-based approach for interpreting genome-wide expression profiles. *Proc. Natl. Acad. Sci. U. S. A.* 102 (43), 15545–15550.
- Swerdlow, R.H., 2020. The mitochondrial hypothesis: dysfunction, bioenergetic defects, and the metabolic link to Alzheimer's disease. *Int. Rev. Neurobiol.* 154, 207–233.
- Szklarczyk, D., Kirsch, R., Koutrouli, M., Nastou, K., Mehryary, F., Hachili, R., Gable, A. L., Fang, T., Doncheva, N.T., Pyysalo, S., Bork, P., Jensen, L.J., von Mering, C., 2023. The STRING database in 2023: protein-protein association networks and functional enrichment analyses for any sequenced genome of interest. *Nucleic Acids Res.* 51 (D1), D638–D646.
- Tang, M.Y., Vranas, M., Krahn, A.I., Pundlik, S., Trempe, J.F., Fon, E.A., 2017. Structure-guided mutagenesis reveals a hierarchical mechanism of Parkin activation. *Nat. Commun.* 8, 14697.
- Therriault, J., Pascoal, T.A., Sefranek, M., Mathotaarachchi, S., Benedet, A.L., Chamoun, M., Lussier, F.Z., Tissot, C., Bellaver, B., Lukasewicz, P.S., Zimmer, E.R., Saha-Chaudhuri, P., Gauthier, S., Rosa-Neto, P., Alzheimer's Disease Neuroimaging, I., 2021. Amyloid-dependent and amyloid-independent effects of tau in individuals without dementia. *Ann. Clin. Transl. Neurol.* 8 (10), 2083–2092.
- Torres, A.K., Jara, C., Olesen, M.A., Tapia-Rojas, C., 2021. Pathologically phosphorylated tau at S396/404 (PHF-1) is accumulated inside of hippocampal synaptic mitochondria of aged wild-type mice. *Sci. Rep.* 11 (1), 4448.
- Tracey, T.J., Steyn, F.J., Wolvetang, E.J., Ngo, S.T., 2018. Neuronal lipid metabolism: multiple pathways driving functional outcomes in health and disease. *Front Mol. Neurosci.* 11, 10.
- Trease, A.J., George, J.W., Roland, N.J., Lichter, E.Z., Emanuel, K., Totusek, S., Fox, H.S., Stauch, K.L., 2022. Hyperphosphorylated human tau accumulates at the synapse, localizing on synaptic mitochondrial outer membranes and disrupting respiration in a mouse model of Tauopathy. *Front Mol. Neurosci.* 15, 852368.
- Trempe, J.F., Sauve, V., Grenier, K., Seifari, M., Tang, M.Y., Menade, M., Al-Abdul-Wahid, S., Krett, J., Wong, K., Kozlov, G., Nagar, B., Fon, E.A., Gehring, K., 2013. Structure of parkin reveals mechanisms for ubiquitin ligase activation. *Science* 340 (6139), 1451–1455.
- Tucker, K.L., Meyer, M., Barde, Y.A., 2001. Neurotrophins are required for nerve growth during development. *Nat. Neurosci.* 4 (1), 29–37.
- Vaseva, A.V., Marchenko, N.D., Ji, K., Tsirka, S.E., Holzmann, S., Moll, U.M., 2012. p53 opens the mitochondrial permeability transition pore to trigger necrosis. *Cell* 149 (7), 1536–1548.
- Villa, E., Marchetti, S., Ricci, J.E., 2018. No Parkin zone: Mitophagy without Parkin. *Trends Cell Biol.* 28 (11), 882–895.
- Vogels, T., Murgoci, A.N., Hromadka, T., 2019. Intersection of pathological tau and microglia at the synapse. *Acta Neuropathol. Commun.* 7 (1), 109.
- Vos, M., Lauwers, E., Verstreken, P., 2010. Synaptic mitochondria in synaptic transmission and organization of vesicle pools in health and disease. *Front Synaptic Neurosci* 2, 139.
- Wu, T., Hu, E., Xu, S., Chen, M., Guo, P., Dai, Z., Feng, T., Zhou, L., Tang, W., Zhan, L., Fu, X., Liu, S., Bo, X., Yu, G., 2021. clusterProfiler 4.0: a universal enrichment tool for interpreting omics data. *Innovation (Camb)* 2 (3), 100141.
- Ye, X., Sun, X., Starovoytov, V., Cai, Q., 2015. Parkin-mediated mitophagy in mutant hAPP neurons and Alzheimer's disease patient brains. *Hum. Mol. Genet.* 24 (10), 2938–2951.
- Yi, W., MacDougall, E.J., Tang, M.Y., Krahn, A.I., Gan-Or, Z., Trempe, J.F., Fon, E.A., 2019. The landscape of Parkin variants reveals pathogenic mechanisms and therapeutic targets in Parkinson's disease. *Hum. Mol. Genet.* 28 (17), 2811–2825.
- Zheng, R., Du, Y., Wang, X., Liao, T., Zhang, Z., Wang, N., Li, X., Shen, Y., Shi, L., Luo, J., Xia, J., Wang, Z., Xu, J., 2022. KIF2C regulates synaptic plasticity and cognition in mice through dynamic microtubule depolymerization. *Elife* 11.
- Zhou, M., Tang, S., 2022. Effect of a dual orexin receptor antagonist on Alzheimer's disease: sleep disorders and cognition. *Front Med (Lausanne)* 9, 984227.